ADVANCED OPTICAL MATERIALS
www.advopticalmat.de

A Comprehensive Multipolar Theory for Periodic Metasurfaces

Aso Rahimzadegan, Theodosios D. Karamanos,* Rasoul Alaee, Aristeidis G. Lamprianidis, Dominik Beutel, Robert W. Boyd, and Carsten Rockstuhl*

Optical metasurfaces consist of 2D arrangements of scatterers, and they control the amplitude, phase, and polarization of an incidence field on demand. Optical metasurfaces are the cornerstone for a future generation of flat optical devices in a wide range of applications. The rapid advances in nanofabrication have made the versatile design and analysis of these ultra-thin surfaces an ever-growing necessity. However, a comprehensive theory to describe the optical response of periodic metasurfaces in closed-form and analytical expressions has not been formulated, and prior attempts are frequently approximate. Here, a theory is developed that analytically links the properties of the scatterer, from which a metasurface is made, to its response via the lattice coupling matrix. The scatterers are represented by their polarizability or T matrix. Explicit expressions for the optical response up to octupolar order in both spherical and Cartesian coordinates are provided, for normal or oblique incidence. Several examples demonstrate that the proposed theoretical approach is a powerful tool for exploring the physics of metasurfaces and designing novel flat optics devices. Novel fully-diffracting metagratings and particle-independent polarization filters are proposed, and novel insights into bound states in the continuum, collective lattice resonances, and the response of Huygens' metasurfaces under oblique incidence are provided.

1. Introduction

During the past decade, research in electromagnetic metamaterials has grown into a solid and mature scientific domain. Their 2D counterparts, metasurfaces, have gained particular attention thanks to their easier fabrication combined with exciting application perspectives at microwave, THz, and optical frequencies.[1–5] Metasurfaces exhibit a plethora of properties, which make them appealing for a wide range of applications, such as absorbers,[6,7] reciprocal and nonreciprocal polarization rotators,[8–10] holograms,[11–16] lenses,[17–21] splitters,[22] diffusers,[23,24] light sails for space explorations,[25,26] biomedical applications,[27] as well as computational and quantum applications.[28,29]

The growing number of metasurface applications and rapid advances in their fabrication and characterization[30] prompt methodologies to accurately analyze and design metasurfaces. While full-wave numerical solutions are always an option, analytical tools can be much more appealing because they facilitate the design and provide valuable insights into the underlying physics of metasurfaces. For periodic metasurfaces that consist of a single scatterer per unit cell, the type of metasurfaces on which we concentrate herein (**Figure 1**), several techniques exist for this purpose. First, comprehensible circuit models of metasurfaces and metamaterials[31–33] were developed, which are easy to use in industry, especially for microwave applications. A second approach follows the homogenization principle. It aims to replace metasurfaces at stake with surfaces with equivalent surface susceptibilities.[34–36] Although very helpful for component design, these methods are inadequate to describe the internal physics of the structures under study, such as the interaction of consisting particles. Moreover, circuit modeling and homogenization methodologies involve, sometimes, assumptions that simplify the investigated problem at the expense of accuracy.

More from "first-principles," a third approach aims to construct the response of 2D arrays from the bottom-up by summing the response of its constituting particles. While sharing some characteristics with the two approaches mentioned initially, this bottom-up approach is more general and versatile. It enables the easier handling of a plethora of designs, including mm-wave and optical applications.[7,37–44] In this approach, the optical action of the constituting particles is best discussed using a multipolar expansion of fields.[45–51] Within the multipolar expansion, the scatterers' optical response is expressed in a series of multipole moments induced by the external illumination and the scattered field from all the other particles forming the metasurface. Using an ever-increasing

A. Rahimzadegan, T. D. Karamanos, R. Alaee, A. G. Lamprianidis, D. Beutel, C. Rockstuhl
Institute of Theoretical Solid State Physics
Karlsruhe Institute of Technology
76131 Karlsruhe, Germany
E-mail: aso.rahimzadegan@kit.edu; theodosios.karamanos@kit.edu

R. Alaee, R. W. Boyd
Department of Physics
University of Ottawa
Ottawa, Ontario K1N 6N5, Canada

C. Rockstuhl
Institute of Nanotechnology
Karlsruhe Institute of Technology
76131 Karlsruhe, Germany

The ORCID identification number(s) for the author(s) of this article can be found under https://doi.org/10.1002/adom.202102059.

DOI: 10.1002/adom.202102059

number of multipole moments is important to capture the response of meta-atoms and consequently the metasurface more accurately. The involved fields are expanded into an orthonormal basis set to reach an algebraic formulation of the scattering process. The amplitude of each mode used to expand the incident and the scattered field is one element of a dedicated vector. The relation between the expansion coefficient of the incident and the scattered field is, then, merely a matrix multiplication. The connecting matrix can then be considered as the most comprehensive representation of the scatterers' optical properties. Two different formulations for this matrix can be found, namely the polarizability matrix and the T matrix.

The polarizability matrix expresses the scattering response in Cartesian coordinates. Several methodologies have been developed to acquire the polarizability matrix beyond simple shapes, especially for the lowest, that is, the dipolar order.[52–54] On the other hand, the T matrix expresses the scattering response in spherical coordinates. It has attracted a substantial share of interest as it can easily accommodate higher-order multipole moments.[55–57] Due to the equivalence of Cartesian and spherical coordinates representations,[58] polarizability and T matrices are interchangeable in the sense that they contain the same information. This equivalence has been explicitly documented up to quadrupolar order,[59] and, more recently, up to octupolar order.[60]

Modeling of metasurfaces via the multipolar analysis initially involved considering particles characterized by only dipole moments,[37] while specific quadrupole moments were added later into the models.[7,61] Moreover, the description of the interaction among all the particles forming the periodic metasurfaces is crucial in every modeling attempt. Earlier works involved approximate expression for this purpose and failed to accurately capture the spatial dispersion occurring in many applications where the metasurfaces are not operated in a deep sub-wavelength regime.[37] Following this observation, efforts shifted into expressing this lattice interaction more accurately, particularly via fast converging Green's function summations.[62] This has resulted in interesting models that could accommodate dipole moments at oblique incidence,[63–66] dipole and quadrupole moments at normal incidence,[67] and even up to octupole moments at normal incidence.[68] However, these efforts were generally limited in scope, for example, focusing on specific particles with specific combinations of multipole moments (i.e., isotropic particles most of the time) or were limited to normal incidence. Furthermore, diffracting metasurfaces were not studied because sub-wavelength metasurfaces were considered that sustain only a zeroth-order mode in reflection and transmission.

To alleviate these problems, D. Beutel et al.[69] used spherical coordinates and a T matrix representation to develop a numerical method to calculate the complete response of a metasurface, that is, propagating and evanescent modes, for any particle and up to a desired multipolar order. Based on previous efforts on isotropic particles,[70,71] this approach employs the Ewald summation[72,73] for the fast-converging determination of the lattice couplings to achieve a complete description of a 2D array response. Although efficient, this work lacks the interchangeability between spherical and more popular-Cartesian representations. It also lacks closed-form analytical expressions, which increases the understanding and versatility among users in physics and engineering.

In this work, we derive accessible expressions for the optical response of periodic metasurfaces to provide a unifying and comprehensive framework. The expressions are based on a multipole expansion and accurately express the amplitudes of propagating diffraction orders of periodic metasurfaces upon illumination at normal or oblique incidence. This approach renders our contribution relevant for the study of metasurfaces and diffracting metagratings. While higher-order multipole moments can be accommodated, we express the response from the scattering structure defining the unit cell of the metasurface up to the octupolar order. Unlike previous attempts, the proposed methodology is interchangeable between a Cartesian and spherical basis, meaning that either the polarizability or T matrix of a particle can be considered, making our contribution flexible, general, and convenient to use. Additionally, we demonstrate reducing our generally valid expressions to handy closed-form analytical formulas for selected specific cases if not all degrees of freedom are accommodated. Such reduction eases physical explorations and simplifies the design. Finally, the robustness of the provided analytical formulas is demonstrated when applying them to selected design challenges for metasurfaces and metagratings.

The paper is structured as follows. The first section defines the multipole moments and fields and provides formulas that transform them between a Cartesian and spherical basis. Additionally, the lattice coupling matrices are defined (**Figure 2** Row I), and the concepts of effective polarizability/T matrices within 2D arrays are elaborated. At the end of this section, closed-form equations to express the optical response from scattering metasurfaces composed of meta-atoms with general symmetries described up to octupolar order and for an arbitrary illumination direction are presented in a Cartesian and vector spherical harmonics basis. Simplified expressions are provided for rectangular and cubic lattices. In the following section, we explore the symmetry of the lattice coupling matrix at the practically most important examples of a square and hexagonal lattice at normal incidence. The isolated and effective polarizability or T matrices of three meta-atoms with distinct symmetries (isotropic, anisotropic, bianisotropic) are explored inside and outside a square/hexagonal lattice.

Afterward, we demonstrate how to reduce the most comprehensive expressions to some special cases and how to use these expressions in specific design challenges. Subsequently, we derive an analytic expression for the amplitudes of the propagating diffraction orders in transmission and reflection from a square-periodic array decorated with isotropic particles described in dipolar–quadrupolar approximation and illuminated at normal incidence. These analytic equations help design a fully diffracting metagrating and predict the spectral locations of bound states in the continuum and collective lattice resonances.

In the last section, we explore obliquely illuminated metasurfaces. We derive an analytic expression for the amplitude of the zeroth-order in transmission and reflection of metasurfaces made from isotropic and dipolar meta-atoms. The analytic equations help to design a particle-independent polarization filter. It also helps to analyze Huygens' metasurfaces[3,74–76] under oblique incidence.

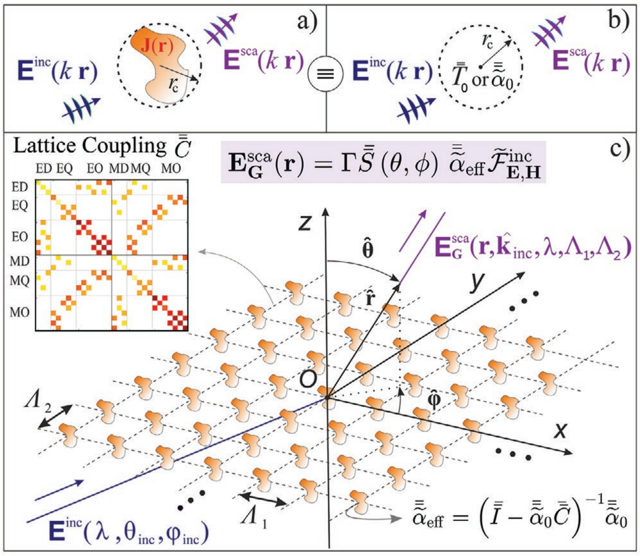

Figure 1. The set-up: a) An arbitrary particle placed into an infinite, homogeneous space, illuminated by an incident wave, $\mathbf{E}^{\text{inc}}$, and its subsequent scattered wave, $\mathbf{E}^{\text{sca}}$. The radius of the smallest sphere enclosing the particle is r_c, while $\mathbf{J}(\mathbf{r})$ is the induced current volume density. b) Equivalent setup as (a) for $r > r_c$, when the respective T or polarizability matrices are used. c) A scattering rectangular 2D lattice of identical scatterers along with the set-up Cartesian and spherical coordinate systems. A simplified equation for the scattered field in Cartesian coordinates is shown in the figure. This response depends on the effective polarizability $\bar{\bar{\tilde{\alpha}}}_{\text{eff}}$, the Cartesian multipole-to-field translation matrix $\bar{\bar{S}}(\theta,\phi)$, and the incident electromagnetic field $\tilde{\mathcal{F}}^{\text{inc}}_{\mathbf{E},\mathbf{H}}$. The effective polarizability is a function of the lattice coupling matrix $\bar{\bar{C}}$ and the polarizability of the isolated particle $\bar{\bar{\tilde{\alpha}}}_0$. The inset shows the lattice coupling for a rectangular lattice. The labels denote the electric (E) and magnetic (M) coupling of dipolar (D), quadrupolar (Q), and octupolar (O) orders.

Finally, the Appendix includes essential derivations and equations, while the Supporting Information includes the step-by-step derivations and complementary information.

2. Multipolar Calculation of the Scattering Field from a 2D Array in Cartesian and Vector Spherical Harmonics Basis: General Equations

2.1. Isolated Particles

Let us consider an arbitrary particle placed in an infinite, homogeneous surrounding, as shown in Figure 1a. In the vector spherical harmonics basis, the scattering response of the particle to an incident electromagnetic wave outside the smallest sphere circumscribing the particle can be described via the T matrix, or $\bar{\bar{T}}_0$, as

$$\begin{bmatrix} \mathbf{b}_1^{\text{e}} \\ \mathbf{b}_2^{\text{e}} \\ \mathbf{b}_3^{\text{e}} \\ \mathbf{b}_1^{\text{m}} \\ \mathbf{b}_2^{\text{m}} \\ \mathbf{b}_3^{\text{m}} \end{bmatrix} = \bar{\bar{T}}_0 \begin{bmatrix} \mathbf{q}_1^{\text{e}} \\ \mathbf{q}_2^{\text{e}} \\ \mathbf{q}_3^{\text{e}} \\ \mathbf{q}_1^{\text{m}} \\ \mathbf{q}_2^{\text{m}} \\ \mathbf{q}_3^{\text{m}} \end{bmatrix} \tag{1a}$$

with

$$\bar{\bar{T}}_0 = \begin{bmatrix} \bar{\bar{T}}_{11}^{\text{ee}} & \bar{\bar{T}}_{12}^{\text{ee}} & \bar{\bar{T}}_{13}^{\text{ee}} & \bar{\bar{T}}_{11}^{\text{em}} & \bar{\bar{T}}_{12}^{\text{em}} & \bar{\bar{T}}_{13}^{\text{em}} \\ \bar{\bar{T}}_{21}^{\text{ee}} & \bar{\bar{T}}_{22}^{\text{ee}} & \bar{\bar{T}}_{23}^{\text{ee}} & \bar{\bar{T}}_{21}^{\text{em}} & \bar{\bar{T}}_{22}^{\text{em}} & \bar{\bar{T}}_{23}^{\text{em}} \\ \bar{\bar{T}}_{31}^{\text{ee}} & \bar{\bar{T}}_{32}^{\text{ee}} & \bar{\bar{T}}_{33}^{\text{ee}} & \bar{\bar{T}}_{31}^{\text{em}} & \bar{\bar{T}}_{32}^{\text{em}} & \bar{\bar{T}}_{33}^{\text{em}} \\ \bar{\bar{T}}_{11}^{\text{me}} & \bar{\bar{T}}_{12}^{\text{me}} & \bar{\bar{T}}_{13}^{\text{me}} & \bar{\bar{T}}_{11}^{\text{mm}} & \bar{\bar{T}}_{12}^{\text{mm}} & \bar{\bar{T}}_{13}^{\text{mm}} \\ \bar{\bar{T}}_{21}^{\text{me}} & \bar{\bar{T}}_{22}^{\text{me}} & \bar{\bar{T}}_{23}^{\text{me}} & \bar{\bar{T}}_{21}^{\text{mm}} & \bar{\bar{T}}_{22}^{\text{mm}} & \bar{\bar{T}}_{23}^{\text{mm}} \\ \bar{\bar{T}}_{31}^{\text{me}} & \bar{\bar{T}}_{32}^{\text{me}} & \bar{\bar{T}}_{33}^{\text{me}} & \bar{\bar{T}}_{31}^{\text{mm}} & \bar{\bar{T}}_{32}^{\text{mm}} & \bar{\bar{T}}_{33}^{\text{mm}} \end{bmatrix} \tag{1b}$$

herein, expressed up to the third (i.e., the octupolar) order. The T matrix represents the electromagnetic response of a scatterer. The scattering coefficient vectors in the vector spherical harmonics (VSH) basis are defined as $\mathbf{b}_j^{\nu} = [b_{j,-j}^{\nu}\ b_{j,-j+1}^{\nu} \ldots b_{j,j-1}^{\nu}\ b_{j,j}^{\nu}]^T$, with ν = {e, m} denoting the electric or magnetic multipoles and j = {1, 2, 3} being the multipolar order corresponding to dipole, quadrupole, and octupole response. The vectors $\mathbf{q}_j^{\nu}$ contain the amplitude coefficients expanding the incident field similarly to the scattering coefficient vectors. The subscript "0" for the T matrix refers to the response of an isolated particle.

Note that VSH functions are defined, herein, as in ref. [47] (Appendix A). Alternatively, the scattering coefficients can be calculated from the scattered field of a particle as defined in Appendix A.

Alternative to the vector spherical harmonics basis, we can also describe the scattering response in the Cartesian basis by a normalized polarizability matrix, or in short, the polarizability matrix, $\bar{\bar{\tilde{\alpha}}}_0$, defined up to the octupolar order through

$$\begin{bmatrix} (\varepsilon\zeta_1)^{-1}\,\mathbf{p} \\ k(\varepsilon\zeta_2)^{-1}\,\mathbf{Q}^{\text{e}} \\ k^2(\varepsilon\zeta_3)^{-1}\,\mathbf{O}^{\text{e}} \\ \mathrm{i}\eta(\zeta_1)^{-1}\,\mathbf{m} \\ \mathrm{i}\eta k(\zeta_2)^{-1}\,\mathbf{Q}^{\text{m}} \\ \mathrm{i}\eta k^2(\zeta_3)^{-1}\,\mathbf{O}^{\text{m}} \end{bmatrix} = \frac{\bar{\bar{\tilde{\alpha}}}_0}{k^3} \tilde{\mathcal{F}}^{\text{inc}}_{\mathbf{E},\mathbf{H}} = \frac{\bar{\bar{\tilde{\alpha}}}_0}{k^3} \begin{bmatrix} \zeta_1 \mathbf{E}_1 \\ k^{-1}\zeta_2 \mathbf{E}_2 \\ k^{-2}\zeta_3 \mathbf{E}_3 \\ \mathrm{i}\eta\zeta_1 \mathbf{H}_1 \\ \mathrm{i}\eta k^{-1}\zeta_2 \mathbf{H}_2 \\ \mathrm{i}\eta k^{-2}\zeta_3 \mathbf{H}_3 \end{bmatrix} \tag{2a}$$

with

$$\bar{\bar{\tilde{\alpha}}}_0 = \begin{bmatrix} \bar{\bar{\tilde{\alpha}}}_{11}^{\text{ee}} & \bar{\bar{\tilde{\alpha}}}_{12}^{\text{ee}} & \bar{\bar{\tilde{\alpha}}}_{13}^{\text{ee}} & \bar{\bar{\tilde{\alpha}}}_{11}^{\text{em}} & \bar{\bar{\tilde{\alpha}}}_{12}^{\text{em}} & \bar{\bar{\tilde{\alpha}}}_{13}^{\text{em}} \\ \bar{\bar{\tilde{\alpha}}}_{21}^{\text{ee}} & \bar{\bar{\tilde{\alpha}}}_{22}^{\text{ee}} & \bar{\bar{\tilde{\alpha}}}_{23}^{\text{ee}} & \bar{\bar{\tilde{\alpha}}}_{21}^{\text{em}} & \bar{\bar{\tilde{\alpha}}}_{22}^{\text{em}} & \bar{\bar{\tilde{\alpha}}}_{23}^{\text{em}} \\ \bar{\bar{\tilde{\alpha}}}_{31}^{\text{ee}} & \bar{\bar{\tilde{\alpha}}}_{32}^{\text{ee}} & \bar{\bar{\tilde{\alpha}}}_{33}^{\text{ee}} & \bar{\bar{\tilde{\alpha}}}_{31}^{\text{em}} & \bar{\bar{\tilde{\alpha}}}_{32}^{\text{em}} & \bar{\bar{\tilde{\alpha}}}_{33}^{\text{em}} \\ \bar{\bar{\tilde{\alpha}}}_{11}^{\text{me}} & \bar{\bar{\tilde{\alpha}}}_{12}^{\text{me}} & \bar{\bar{\tilde{\alpha}}}_{13}^{\text{me}} & \bar{\bar{\tilde{\alpha}}}_{11}^{\text{mm}} & \bar{\bar{\tilde{\alpha}}}_{12}^{\text{mm}} & \bar{\bar{\tilde{\alpha}}}_{13}^{\text{mm}} \\ \bar{\bar{\tilde{\alpha}}}_{21}^{\text{me}} & \bar{\bar{\tilde{\alpha}}}_{22}^{\text{me}} & \bar{\bar{\tilde{\alpha}}}_{23}^{\text{me}} & \bar{\bar{\tilde{\alpha}}}_{21}^{\text{mm}} & \bar{\bar{\tilde{\alpha}}}_{22}^{\text{mm}} & \bar{\bar{\tilde{\alpha}}}_{23}^{\text{mm}} \\ \bar{\bar{\tilde{\alpha}}}_{31}^{\text{me}} & \bar{\bar{\tilde{\alpha}}}_{32}^{\text{me}} & \bar{\bar{\tilde{\alpha}}}_{33}^{\text{me}} & \bar{\bar{\tilde{\alpha}}}_{31}^{\text{mm}} & \bar{\bar{\tilde{\alpha}}}_{32}^{\text{mm}} & \bar{\bar{\tilde{\alpha}}}_{33}^{\text{mm}} \end{bmatrix} \tag{2b}$$

$$\zeta_j = \sqrt{(2j+1)!\pi} \tag{2c}$$

where $k = 2\pi/\lambda$ is the wavenumber of the scattered field in the embedding medium, $\eta = \sqrt{\mu/\varepsilon}$ is the impedance of the embedding medium, ε and μ are the permittivity and permeability of the embedding medium, respectively, and $\tilde{\mathcal{F}}^{\text{inc}}_{\mathbf{E},\mathbf{H}}$ is the

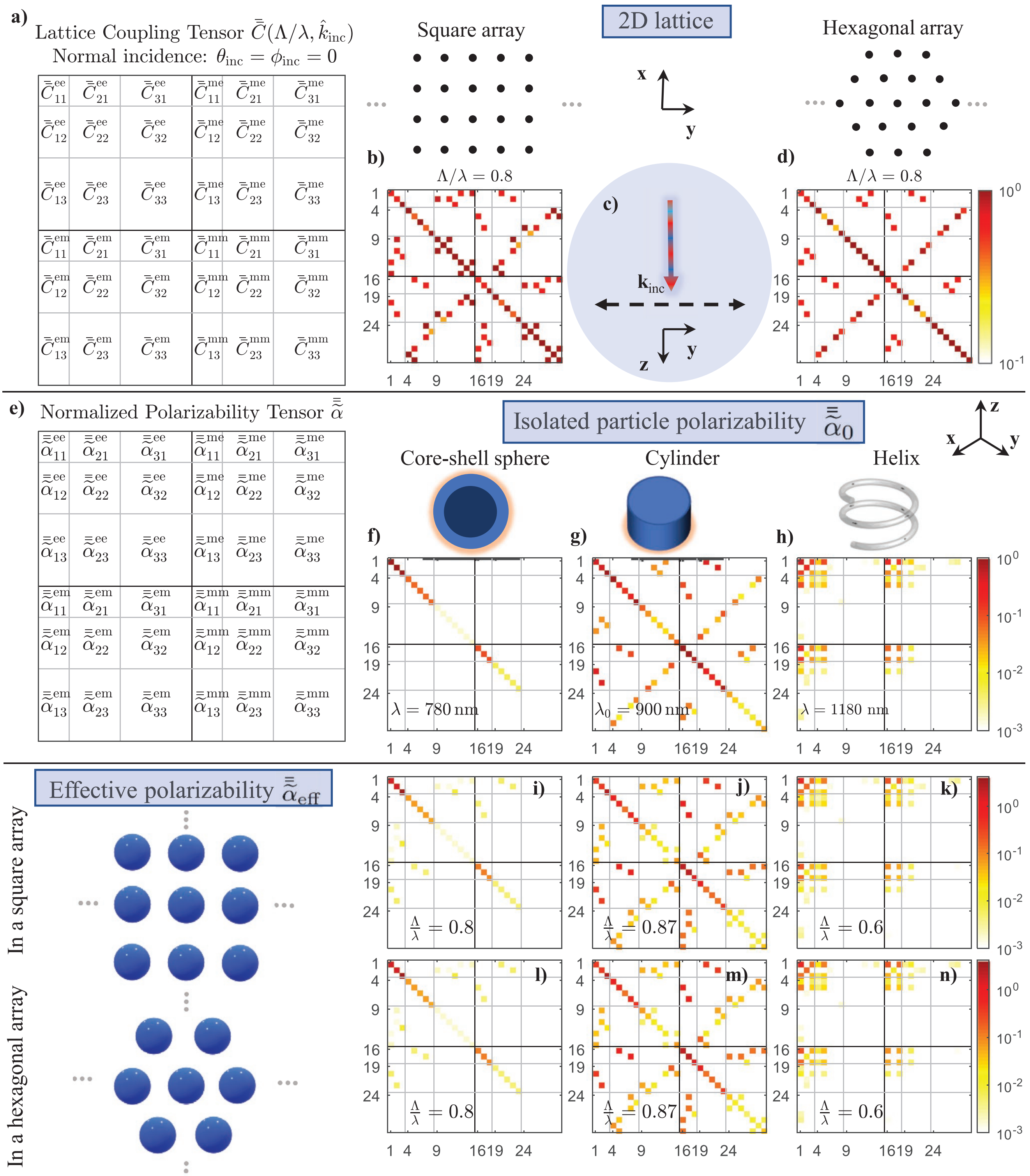

Figure 2. Symmetries of scatterers and 2D lattices in Cartesian basis: Row I: a) The Cartesian lattice coupling matrix amplitude up to octupolar order for b) a square array and d) a hexagonal array under normal incidence (i.e., $\theta_{inc} = 0$), as shown in (c). The normalized periodicity $\hat{\Lambda}$ for both arrays is 0.8. Row II: e) The normalized polarizability matrix amplitude for f) an isolated Ag-core SiO_2-shell particle ($r_{core} = 120$ nm, $r_{shell} = 120 + 30$ nm) in free space at $\lambda = 780$ nm, and g) an isolated amorphous silicon ($n = 3.959 + 0.009i$) cylinder ($r = 291$ nm, $h = 211$ nm) embedded in silica ($n = 1.44$) at $\lambda_0 = 900$ nm, and h) an isolated silver ($n = 0.095 + 8.675i$[78]) helix ($R_{axial} = 80$ nm, $r_{rod} = 20$ nm, $P_{pitch} = 105$ nm, and $N_{turn} = 2$) in free space at $\lambda = 1180$ nm. Row III: The normalized effective polarizability amplitude of i, j) the core-shell sphere, j,m) the cylinder, and k,n) the helix inside an infinitely periodic i–k) square array or l–n) hexagonal array.

normalized electromagnetic incident field. The tilde indicates the normalized polarizability (Appendix B). This dimensionless and irreducible polarizability matrix $\tilde{\bar{\bar{\alpha}}}_0$ facilitates analytic calculations and will simplify equations later on in this work. The vectors $\mathbf{E}_n$ and $\mathbf{H}_n$ are the electric and magnetic multipolar amplitudes of the incident field as defined in Appendix B, and contain spatial derivatives of the Cartesian incident fields at the origin considered as the center of the particle.[59,60,77] The vectors $\mathbf{p}$ ($\mathbf{m}$), $\mathbf{Q}^{\mathrm{e}}$ ($\mathbf{Q}^{\mathrm{m}}$), and $\mathbf{O}^{\mathrm{e}}$ ($\mathbf{O}^{\mathrm{m}}$), are the irreducible Cartesian electric (magnetic) dipole, quadrupole, and octupole moments, respectively (Appendix C). The far-fields radiated by a scattering particle as a function of the multipole moments expressed in Cartesian basis are also provided in Appendix D.

If we employ the transformation formulas, we can acquire the elements of the T matrix from the ones of the polarizability matrix and vice versa via

$$\bar{\bar{T}}_{jj'}^{\nu\nu'} = \mathrm{i}\bar{\bar{F}}_j^{-1}\,\tilde{\bar{\bar{\alpha}}}_{jj'}^{\nu\nu'}\,\bar{\bar{F}}_{j'} \tag{3a}$$

$$\tilde{\bar{\bar{\alpha}}}_{jj'}^{\nu\nu'} = -\mathrm{i}\,\bar{\bar{F}}_j\,\bar{\bar{T}}_{jj'}^{\nu\nu'}\,\bar{\bar{F}}_{j'}^{-1} \tag{3b}$$

where $\{j, j'\} = \{1, 2, 3\}$ and $\{\nu,\nu'\}=\{\mathrm{e},\mathrm{m}\}$. The expressions do not have a subscript "0" as they are valid for the particles independent of whether we consider them isolated in free space or as a part of the lattice. In this work, the use of the normalized polarizability matrix and the choice of transformer tensors such that $\bar{\bar{F}}_j = \left(\bar{\bar{F}}_j^{-1}\right)^{\dagger}$ (Appendix E) enabled the formulation of simpler formulas than the case of ref. [60]. This has become possible by defining, herein, the multipole and the fields in Cartesian coordinates as provided in Appendix C. Therefore, a scattering particle can be described either in the Cartesian or the vector spherical harmonics basis and be replaced by the respective T or polarizability matrix, as depicted in Figure 1b, simplifying, subsequently, the analysis extensively.

The normalized polarizability matrix of three objects with three different symmetries (spherical, cylindrical, and helical) are shown up to octupolar order in Figure 2 Row II. For the interested reader and completeness, the vector spherical harmonics counterpart of the figure is plotted in Figure S3, Supporting Information. While analytical solutions for the polarizability of isotropic particles are available via the Mie theory, the polarizability of the nonspherical particles has been obtained from full-wave numerical simulations based on the finite-element method as described in Appendix A. These numerical simulations are the only full-wave simulations involved in our analysis. They constitute the base, as they provide information on how a single particle scatters light. Nevertheless, once it is calculated and stored, it can be reused in all future calculations that consider the same particle.

An isotropic particle (Figure 2f) has a diagonal T and polarizability matrix. The diagonal elements of the T matrix are the Mie coefficients, but with a negative sign, in agreement with the definitions of VSH (Appendix A). The diagonal elements of the normalized polarizability are the Mie coefficients with an "i" multiplicand. Unlike isotropic particles, a particle with cylindrical symmetry (Figure 2g) only has a diagonal polarizability matrix for the dipolar order. Beyond dipolar approximation, nondiagonal terms appear, which need to be taken into account. For helical structures (Figure 2h) that possess a chiral response, nonzero terms exist in the diagonal of the electric-magnetic polarizability matrices. Note that the white elements in the matrices in Figure 2 Row II are either symmetry-protected strictly zero or express a diminishing response of the small particle for higher multipolar orders. Especially these symmetry-protected zeros are important, as they help construct a theoretical model up to a particular multipolar order and for a specific particle symmetry that leads to simplified analytical equations for the metasurface scattering response. We can ignore them from the very first beginning. The symmetry of the normalized polarizability or the T matrix within the defined bases fully describes the electromagnetic symmetry and response of a particle. This feature makes these two matrices crucial tools in nanophotonics design and analysis.

So far, we have focused on the response of isolated particles. The following subsection explores how these polarizabilities/T matrices are modified inside a 2D lattice and how to derive such effective matrices analytically.

2.2. Periodic Arrangement of Identical Particles

Let us assume an infinite number of arbitrary, but identical particles arranged in a 2D lattice described by two unit-cell base vectors, $\mathbf{u}_1$ and $\mathbf{u}_2$, parallel to the lattice plane,[79] with $|\mathbf{u}_1| = \Lambda_1$ and $|\mathbf{u}_2| = \Lambda_2$ being the two periodicities (Figure 1c). The arrangement is embedded in a homogeneous material with refractive index $n = \sqrt{\varepsilon_{\mathrm{r}}\mu_{\mathrm{r}}}$, with ε_{r} and μ_{r} being the relative permittivity and permeability of the medium, respectively.

Now, let us assume that the 2D lattice is illuminated by a time-harmonic plane electromagnetic wave with an electric field corresponding to $\mathbf{E}^{\mathrm{inc}} = \mathbf{E}_0 e^{\mathrm{i}\mathbf{k}^{\mathrm{inc}}\cdot\mathbf{r}}$, with $\mathbf{k}^{\mathrm{inc}}(\theta_{\mathrm{inc}},\phi_{\mathrm{inc}},\lambda) = k_0 n(\hat{\mathbf{k}}_{\mathrm{inc}}\cdot\hat{\mathbf{r}}) = k_x^{\mathrm{inc}}\,\hat{\mathbf{x}} + k_y^{\mathrm{inc}}\,\hat{\mathbf{y}} + k_z^{\mathrm{inc}}\,\hat{\mathbf{z}}$ being the incident field wavevector and $E_0 = |\mathbf{E}_0|$ being the amplitude of the incident plane wave, which, in this work, is normalized, that is, $E_0 = 1$ V/m unless explicitly mentioned. Note that $\lambda = \lambda_0/n$ is the wavelength inside the embedding medium.

2.2.1. Vector Spherical Harmonics Basis

For the case of the spherical coordinate, the general equation for the amplitude of each diffraction order propagating in a medium without absorption and supported by the reciprocal lattice $\mathbf{G}$, can be derived as[80] (Sections S.I.A and S.I.B, Supporting Information)

$$\mathbf{E}_{\mathrm{s},\mathbf{G}}^{\mathrm{sca}}(\mathbf{r}) = \begin{bmatrix} E_{\mathbf{G},\theta}^{\mathrm{sca}}(\mathbf{r}) \\ E_{\mathbf{G},\phi}^{\mathrm{sca}}(\mathbf{r}) \end{bmatrix} = \frac{\mathrm{i}\sqrt{\pi}}{2Ak^2}\frac{e^{\mathrm{i}\mathbf{k}_{\mathbf{G}}^{\pm}\cdot\mathbf{r}}}{|\cos\theta|}\sum_{j=1}^{3}\frac{\sqrt{2j+1}}{\mathrm{i}^j}\bar{\bar{W}}_j(\theta,\phi)\begin{bmatrix}\mathbf{b}_j^{\mathrm{e}} \\ \mathbf{b}_j^{\mathrm{m}}\end{bmatrix} \tag{4}$$

where $A = (\mathbf{u}_1 \times \mathbf{u}_2)\cdot\hat{\mathbf{z}}$ is the area of the unit cell, $\mathbf{k}_{\mathbf{G}}^{\pm}$ is the wavevector of the diffraction order of the lattice $\mathbf{G}$, and (θ, ϕ) are the polar and azimuth angles of the wavevector. The "+" and "−" signs refer to forward (i.e., $0 \leqslant \theta \leqslant \pi/2$) and backward (i.e., $\pi/2 < \theta \leqslant \pi$) propagating diffraction orders, respectively.

It corresponds to transmission and reflection. The matrix $\overline{\overline{W}}(\theta,\phi)$ is the spherical multipole-field translation matrix, depending only on the direction of the diffraction order, and contains trigonometric functions. We have calculated its elements as analytic relations up to octupolar order. These elements are provided in Appendix F. These analytic formulas facilitate the derivation of closed-form equations beyond the complexity of the semianalytic, summation approach of Equation (4).

The vectors $\mathbf{b}_j^{\mathrm{e}}$ and $\mathbf{b}_j^{\mathrm{m}}$ in Equation (4) are the effective electric and magnetic scattering coefficients of each of the particles, respectively. They include the interaction among all the particles in the array and are identical for all the (identical) particles due to symmetry. These effective parameters are calculated via Equation (1) by replacing the T matrix of the isolated particle, or $\overline{\overline{T}}_0$, with the effective T matrix calculated via the following equation[81]

$$\overline{\overline{T}}_{\mathrm{eff}}=\left[\overline{\overline{I}}-\overline{\overline{T}}_0(\lambda)\overline{\overline{C}}_s\left(\hat{\mathbf{k}}_{\mathrm{inc}},\frac{\Lambda_1}{\lambda},\frac{\Lambda_2}{\lambda}\right)\right]^{-1}\overline{\overline{T}}_0(\lambda) \tag{5}$$

where $\overline{\overline{I}}$ is the identity matrix, and $\overline{\overline{C}}_s$ is the lattice coupling matrix expressed in spherical coordinates, which is a function of the normalized periodicities $\tilde{\Lambda}$, that is, the physical periodicity normalized to the wavelength, and the direction of illumination. The coupling matrix elements are infinite summations over lattice points and can be calculated using various summation methods for the translation matrices[47,82] (Section S.I.C, Supporting Information). To solve these tedious summations efficiently, we divide them into summations in the real and Fourier space using Ewald's method, which results in exponentially convergent summations.[69] Note that no approximation is used here, up to the considered multipolar order, unlike other references that take approximated Green function summations.

For the specific case of rectangular lattices, like the one depicted in Figure 1c, $\mathbf{k}_{\mathbf{G}}^{\pm}$ of the respective diffraction orders are calculated as[63,80]

$$\mathbf{k}_{\mathbf{G}}^{\pm}=k_{\mathbf{G},x}\,\hat{\mathbf{x}}+k_{\mathbf{G},y}\,\hat{\mathbf{y}}+k_{\mathbf{G},z}^{\pm}\,\hat{\mathbf{z}} \tag{6a}$$

with

$$k_{\mathbf{G},x}=k_x^{\mathrm{inc}}+\frac{2\pi n_1}{\Lambda_1},\quad k_{\mathbf{G},y}=k_y^{\mathrm{inc}}+\frac{2\pi n_2}{\Lambda_2} \tag{6b}$$

$$k_{\mathbf{G},z}^{\pm}=k\cos\theta=k_0 n\cos\theta=\\=\pm\sqrt{k^2-\left(k_x^{\mathrm{inc}}+\frac{2\pi n_1}{\Lambda_1}\right)^2-\left(k_y^{\mathrm{inc}}+\frac{2\pi n_2}{\Lambda_2}\right)^2} \tag{6c}$$

and

$$\cos\theta=\frac{k_{\mathbf{G},z}^{\pm}}{|\mathbf{k}_{\mathbf{G}}^{\pm}|},\quad \phi=\arctan\left(\frac{k_{\mathbf{G},y}}{k_{\mathbf{G},x}}\right) \tag{6d}$$

where $n_1,n_2\in\mathbb{Z}$ are the diffraction orders. Note that the diffraction orders are propagating only if $k_{\mathbf{G},z}^{\pm}\in\mathbb{R}$. A similar procedure can be used to calculate the wavevector $\mathbf{k}_{\mathbf{G}}^{\pm}$ for other types of lattices, for example, hexagonal, as elaborated in the Section S.II, Supporting Information.

2.2.2. Cartesian Basis

The formulations mentioned above in spherical coordinates can be translated into Cartesian coordinates. After employing Equation (E1) and applying the transformations to Cartesian coordinates, expressed in Equation (4), and after tedious calculations, we arrive at (Sections S.I.A and S.I.B, Supporting Information)

$$\mathbf{E}_{\mathrm{c},\mathbf{G}}^{\mathrm{sca}}(\mathbf{r})=\frac{\mathrm{i}k\sqrt{\pi}\mathrm{e}^{\mathrm{i}\mathbf{k}_{\mathbf{G}}^{\pm}\cdot\mathbf{r}}}{2A|\cos\theta|}\overline{\overline{S}}(\theta,\phi)\begin{bmatrix}(\varepsilon\zeta_1)^{-1}\,\mathbf{p}\\ k(\varepsilon\zeta_2)^{-1}\,\mathbf{Q}^{\mathrm{e}}\\ k^2(\varepsilon\zeta_3)^{-1}\,\mathbf{O}^{\mathrm{e}}\\ \mathrm{i}\eta(\zeta_1)^{-1}\,\mathbf{m}\\ \mathrm{i}\eta k(\zeta_2)^{-1}\,\mathbf{Q}^{\mathrm{m}}\\ \mathrm{i}\eta k^2(\zeta_3)^{-1}\,\mathbf{O}^{\mathrm{m}}\end{bmatrix}=\\=\frac{\mathrm{i}\sqrt{\pi}\mathrm{e}^{\mathrm{i}\mathbf{k}_{\mathbf{G}}^{\pm}\cdot\mathbf{r}}}{2Ak^2|\cos\theta|}\overline{\overline{S}}(\theta,\phi)\overline{\overline{\tilde{\alpha}}}_{\mathrm{eff}}\begin{bmatrix}\zeta_1\mathbf{E}_1\\ k^{-1}\zeta_2\mathbf{E}_2\\ k^{-2}\zeta_3\mathbf{E}_3\\ \mathrm{i}\eta\zeta_1\mathbf{H}_1\\ \mathrm{i}\eta k^{-1}\zeta_2\mathbf{H}_2\\ \mathrm{i}\eta k^{-2}\zeta_3\mathbf{H}_3\end{bmatrix} \tag{7}$$

with $\mathbf{E}_{\mathrm{c},\mathbf{G}}^{\mathrm{sca}}(\mathbf{r})=[E_{\mathbf{G},x}^{\mathrm{sca}}\ E_{\mathbf{G},y}^{\mathrm{sca}}\ E_{\mathbf{G},z}^{\mathrm{sca}}]^T$. The matrix $\overline{\overline{S}}(\theta,\phi)$ is the Cartesian multipole-to-field translation matrix, defined as

$$\overline{\overline{S}}(\theta,\phi)=\begin{bmatrix}\mathbf{S}_1^{\mathrm{xe}} & \mathbf{S}_2^{\mathrm{xe}} & \mathbf{S}_3^{\mathrm{xe}} & \mathbf{S}_1^{\mathrm{xm}} & \mathbf{S}_2^{\mathrm{xm}} & \mathbf{S}_3^{\mathrm{xm}}\\ \mathbf{S}_1^{\mathrm{ye}} & \mathbf{S}_2^{\mathrm{ye}} & \mathbf{S}_3^{\mathrm{xe}} & \mathbf{S}_1^{\mathrm{ym}} & \mathbf{S}_2^{\mathrm{ym}} & \mathbf{S}_3^{\mathrm{ym}}\\ \mathbf{S}_1^{\mathrm{ze}} & \mathbf{S}_2^{\mathrm{ze}} & \mathbf{S}_3^{\mathrm{ze}} & \mathbf{S}_1^{\mathrm{zm}} & \mathbf{S}_2^{\mathrm{zm}} & \mathbf{S}_3^{\mathrm{zm}}\end{bmatrix} \tag{8a}$$

with the vector elements of the matrix

$$\mathbf{S}_j(\theta,\phi)=\begin{bmatrix}\mathbf{S}_j^{\mathrm{xe}} & \mathbf{S}_j^{\mathrm{xm}}\\ \mathbf{S}_j^{\mathrm{ye}} & \mathbf{S}_j^{\mathrm{ym}}\\ \mathbf{S}_j^{\mathrm{ze}} & \mathbf{S}_j^{\mathrm{zm}}\end{bmatrix}=\\=\frac{\sqrt{2j+1}}{\mathrm{i}^{1-j}}\left[\overline{\overline{R}}(\theta,\phi)^T\,\overline{\overline{W}}(\theta,\phi)\right]\overline{\overline{F}}_j^{-1} \tag{8b}$$

The $\overline{\overline{R}}(\theta,\phi)$ matrix is the transformation operator from spherical to Cartesian coordinates (Appendix F). The matrix $\overline{\overline{\tilde{\alpha}}}_{\mathrm{eff}}$ in Equation (7) is the normalized effective polarizability matrix. The matrix includes the coupling between particles on the lattice, in the same way as $\overline{\overline{T}}_{\mathrm{eff}}$, as explained above. The effective polarizability can either be calculated from the $\overline{\overline{T}}_{\mathrm{eff}}$ via applying the transformations of Equation (3), or directly via (Section S.VIII, Supporting Information)

$$\overline{\overline{\tilde{\alpha}}}_{\mathrm{eff}}=\left[\overline{\overline{I}}-\overline{\overline{\tilde{\alpha}}}_0(\lambda)\overline{\overline{C}}\left(\hat{\mathbf{k}}_{\mathrm{inc}},\frac{\Lambda_1}{\lambda},\frac{\Lambda_2}{\lambda}\right)\right]^{-1}\overline{\overline{\tilde{\alpha}}}_0(\lambda) \tag{9}$$

where $\overline{\overline{\tilde{\alpha}}}_0$ is the normalized polarizability matrix of the isolated particle and $\overline{\overline{C}}=\mathrm{i}\overline{\overline{F}}\,\overline{\overline{C}}_s\overline{\overline{F}}^{-1}$ is the lattice coupling matrix expressed in Cartesian coordinates. The matrix $\overline{\overline{C}}$ can be, alternatively, calculated using various summation methods for dyadic Green's functions, and, hence, some elements of $\overline{\overline{C}}$ have been analytically obtained.[37,38,62] However, only certain simplified metasurface cases are investigated in these publications, or an approximated Green's function is considered.

Therefore, with the closed-form formulas (4) and (7), introduced in this work, one can effectively calculate the response of a 2D lattice of particles up to octupolar order when illuminated by a plane wave. In particular, Equation (7) that employs Cartesian coordinates, which enjoy popularity in the metasurface community, is a notable contribution.[63,67,83–85] However, we want to point out that both representations, spherical or Cartesian, are physically equivalent,[58] and the choice depends on the geometry of the problem or the user comfort.

The lattice coupling matrix expressed in Cartesian coordinates, $\overline{\overline{C}}$, has the exact dimensions as the polarizability matrix and is defined as

$$\overline{\overline{C}} = \begin{bmatrix} \overline{\overline{C}}_{11}^{\mathrm{ee}} & \overline{\overline{C}}_{12}^{\mathrm{ee}} & \overline{\overline{C}}_{13}^{\mathrm{ee}} & \overline{\overline{C}}_{11}^{\mathrm{em}} & \overline{\overline{C}}_{12}^{\mathrm{em}} & \overline{\overline{C}}_{13}^{\mathrm{em}} \\ \overline{\overline{C}}_{21}^{\mathrm{ee}} & \overline{\overline{C}}_{22}^{\mathrm{ee}} & \overline{\overline{C}}_{23}^{\mathrm{ee}} & \overline{\overline{C}}_{21}^{\mathrm{em}} & \overline{\overline{C}}_{22}^{\mathrm{em}} & \overline{\overline{C}}_{23}^{\mathrm{em}} \\ \overline{\overline{C}}_{31}^{\mathrm{ee}} & \overline{\overline{C}}_{32}^{\mathrm{ee}} & \overline{\overline{C}}_{33}^{\mathrm{ee}} & \overline{\overline{C}}_{31}^{\mathrm{em}} & \overline{\overline{C}}_{32}^{\mathrm{em}} & \overline{\overline{C}}_{33}^{\mathrm{em}} \\ \overline{\overline{C}}_{11}^{\mathrm{me}} & \overline{\overline{C}}_{12}^{\mathrm{me}} & \overline{\overline{C}}_{13}^{\mathrm{me}} & \overline{\overline{C}}_{11}^{\mathrm{mm}} & \overline{\overline{C}}_{12}^{\mathrm{mm}} & \overline{\overline{C}}_{13}^{\mathrm{mm}} \\ \overline{\overline{C}}_{21}^{\mathrm{me}} & \overline{\overline{C}}_{22}^{\mathrm{me}} & \overline{\overline{C}}_{23}^{\mathrm{me}} & \overline{\overline{C}}_{21}^{\mathrm{mm}} & \overline{\overline{C}}_{22}^{\mathrm{mm}} & \overline{\overline{C}}_{23}^{\mathrm{mm}} \\ \overline{\overline{C}}_{31}^{\mathrm{me}} & \overline{\overline{C}}_{32}^{\mathrm{me}} & \overline{\overline{C}}_{33}^{\mathrm{me}} & \overline{\overline{C}}_{31}^{\mathrm{mm}} & \overline{\overline{C}}_{32}^{\mathrm{mm}} & \overline{\overline{C}}_{33}^{\mathrm{mm}} \end{bmatrix} \tag{10}$$

where due to electromagnetic duality symmetry[86–89] $\overline{\overline{C}}_{jj'}^{\mathrm{ee}} = \overline{\overline{C}}_{jj'}^{\mathrm{mm}}$ and $\overline{\overline{C}}_{jj'}^{\mathrm{me}} = \overline{\overline{C}}_{jj'}^{\mathrm{em}}$. Generally, based on the 2D lattice symmetry and incidence angle, the coupling matrices take different arrangements. Specifically, at normal incidence, that is, $\theta_{\mathrm{inc}} = 0$, the coupling matrix takes a much simpler form. Hence, in Figure 2, we show the Cartesian coupling matrix $\overline{\overline{C}}$ for square and hexagonal lattices. The spherical coupling matrix counterpart is shown in Figure S3, Supporting Information. Note that the coupling matrix is a function of the $\hat{\mathbf{k}}_{\mathrm{inc}}$. Therefore, for normal incidence, the choice of ϕ_{inc} does not make any difference. Throughout the manuscript, normal incidence refer to $\theta_{\mathrm{inc}} = 0$, unless, explicitly, a constraint on ϕ_{inc} is mentioned.

Following the calculation of $\overline{\overline{C}}$ for a specific lattice, the normalized effective polarizability can, then, be obtained via Equation (9). The Row III of the Figure 2 shows $\overline{\overline{\tilde{\alpha}}}_{\mathrm{eff}}$ of the spherical, cylindrical, and helical particles inside the square and hexagonal lattices, that is, including the coupling influence of all particles on the 2D array.

Let us now explore a commonly considered case for metasurfaces, the square lattice, with $\Lambda_1 = \Lambda_2 = \Lambda$ as the periodicity. If we calculate the coupling matrix for this case and, afterward, the effective polarizability via Equation (9), the scattered field in Equation (7) is further simplified to

$$\mathbf{E}_{\mathbf{G},\mathrm{c}}^{\mathrm{sca}}\left(\mathbf{r}, \hat{\mathbf{k}}_{\mathrm{inc}}, \tilde{\Lambda}, \lambda\right) = \frac{\mathrm{i}e^{\mathrm{i}\mathbf{k}_{\mathbf{G}}^{\pm}\cdot\mathbf{r}}}{8\pi^{3/2}\,|\cos\theta|\,\tilde{\Lambda}^2}\overline{\overline{S}}(\theta,\phi)\frac{\overline{\overline{\tilde{\alpha}}}_0(\lambda)}{\overline{\overline{I}} - \overline{\overline{\tilde{\alpha}}}_0(\lambda)\overline{\overline{C}}\left(\hat{\mathbf{k}}_{\mathrm{inc}}, \tilde{\Lambda}\right)}\begin{bmatrix} \zeta_1 \mathbf{E}_1\left(\hat{\mathbf{k}}_{\mathrm{inc}}, \lambda\right) \\ k^{-1}\zeta_2 \mathbf{E}_2\left(\hat{\mathbf{k}}_{\mathrm{inc}}, \lambda\right) \\ k^{-2}\zeta_3 \mathbf{E}_3\left(\hat{\mathbf{k}}_{\mathrm{inc}}, \lambda\right) \\ \mathrm{i}\eta\zeta_1 \mathbf{H}_1\left(\hat{\mathbf{k}}_{\mathrm{inc}}, \lambda\right) \\ \mathrm{i}\eta k^{-1}\zeta_2 \mathbf{H}_2\left(\hat{\mathbf{k}}_{\mathrm{inc}}, \lambda\right) \\ \mathrm{i}\eta k^{-2}\zeta_3 \mathbf{H}_3\left(\hat{\mathbf{k}}_{\mathrm{inc}}, \lambda\right) \end{bmatrix} \tag{11}$$

Here, we have included all the arguments in the equation for clarity. The factors that control the response of the particle square array are evident from Equation (11); specifically, the surrounding material, represented by $k = 2\pi n/\lambda_0$, the incident field direction, represented by the field vector and $\hat{\mathbf{k}}_{\mathrm{inc}}$, the properties of the individual particle, represented by $\overline{\overline{\tilde{\alpha}}}_0$, and the dimensions of the lattice, represented by $\tilde{\Lambda}$. Hence, modifying each of these parameters could change the response of the metasurface according to one's goals. As inserting the arguments in Equation (11), can make the equations lengthy and might distract the reader, we ignore them from now on unless needed. However, implicitly they are always assumed.

The summations (4) and (7) can describe the diffracted field from any 2D array in spherical and Cartesian coordinates, respectively, in terms of the incident fields, the lattice, and the consisting particles attributes, provided that the problem can be sufficiently described with octupoles as the maximum multipolar order. Moreover, unlike previous efforts,[38,63] these formulas include all the propagating, diffraction orders and not only a zeroth-order. It allows the study of metagratings operating at wavelengths shorter than the array periodicity and further facilitates the design of related optical structures, as demonstrated later. For convenience, we provide a summary of these equations in **Table 1**. The verification of the proposed equations is performed in the Section S.I.D, Supporting Information. using COMSOL Multiphysics[90] for an isotropic particle, as well as a particle with broken symmetries, namely a metallic helix, and under oblique incidence. The T matrix of the metallic helix was obtained via an extraction algorithm[56] using JCMsuite.[91] The proposed methodology, which employs the multipolar expansion, could produce accurate results that require fewer computational resources in comparison with numerical methods, as similarly reported in ref. [69], provided that the order of expansion is correctly selected.

It should be noted that the form of the matrices and their subsequent symmetries are essentially dependent on the combinations we choose as an irreducible representation of the Cartesian multipole moments and, subsequently, the selection of the transformation matrices $\overline{\overline{F}}_j$, $j = \{1,2,3\}$ (Appendix E). The utilization of the specific transformation matrices, in this work, originates from real spherical harmonic corresponding to atomic orbitals, *p*, *d*, and *f*,[92] and enable the conservation of certain symmetries between Cartesian and spherical bases, such as diagonality for T matrices for isotropic particles. Different setups of multipole moments in Cartesian basis or a different choice of transformation matrices will lead to different matrices in Cartesian basis from those demonstrated in Figure 2, as shown in ref. [60]. Additionally, the polarizability matrix via a different Cartesian basis can be retrieved from the current one through simple algebraic transformations (Section S.IV, Supporting Information).

The multipolar formulation used herein to describe the response of a metasurface composed of identical particles can also be utilized to obtain the resonant modes of this metasurface. This approach, previously applied to 1D chains of particles,[93–95] can analogously be expanded to 2D arrays. Specifically, after the effective multipole moments in the 2D array are written by inserting the effective T matrix of Equation (5) into Equation (1), if the driving field is set to zero or $\mathbf{q}_i^{\mathrm{e,m}} = \mathbf{0}$,

Table 1. Main equations for the scattering of 2D lattices in spherical and Cartesian coordinates.

Spherical[a)]	Conversion	Cartesian[a)]
$\begin{bmatrix} E^{\mathrm{sca}}_{\mathrm{G},\theta} \\ E^{\mathrm{sca}}_{\mathrm{G},\phi} \end{bmatrix} = \Gamma \sum_{j=1}^{3} \frac{\sqrt{2j+1}}{\mathrm{i}^{j}} \bar{\bar{W}}_j \begin{bmatrix} \mathrm{b}^{\mathrm{e}}_j \\ \mathrm{b}^{\mathrm{m}}_j \end{bmatrix}$	$\mathrm{S}_j = \frac{\sqrt{2j+1}}{\mathrm{i}^{1-j}} (\bar{\bar{R}}^{T} \bar{\bar{W}}_j)\, \bar{\bar{F}}_j^{-1}$	$\begin{bmatrix} E^{\mathrm{sca}}_{\mathrm{G},x} \\ E^{\mathrm{sca}}_{\mathrm{G},y} \\ E^{\mathrm{sca}}_{\mathrm{G},z} \end{bmatrix} = \Gamma k^3 \bar{\bar{S}} \begin{bmatrix} \zeta_1^{-1}\varepsilon^{-1}\mathrm{p} \\ \frac{k}{\zeta_2\varepsilon}\mathrm{Q}^{\mathrm{e}} \\ \frac{k^2}{\zeta_3\varepsilon}\mathrm{O}^{\mathrm{e}} \\ \frac{\mathrm{i}\eta}{\zeta_1}\mathrm{m} \\ \frac{\mathrm{i}k\eta}{\zeta_2}\mathrm{Q}^{\mathrm{m}} \\ \frac{\mathrm{i}k^2\eta}{\zeta_3}\mathrm{O}^{\mathrm{m}} \end{bmatrix}$
$\begin{bmatrix} \mathrm{b}^{\mathrm{e}}_1 \\ \mathrm{b}^{\mathrm{e}}_2 \\ \mathrm{b}^{\mathrm{e}}_3 \\ \mathrm{b}^{\mathrm{m}}_1 \\ \mathrm{b}^{\mathrm{m}}_2 \\ \mathrm{b}^{\mathrm{m}}_3 \end{bmatrix} = \bar{\bar{T}} \begin{bmatrix} \mathrm{q}^{\mathrm{e}}_1 \\ \mathrm{q}^{\mathrm{e}}_2 \\ \mathrm{q}^{\mathrm{e}}_3 \\ \mathrm{q}^{\mathrm{m}}_1 \\ \mathrm{q}^{\mathrm{m}}_2 \\ \mathrm{q}^{\mathrm{m}}_3 \end{bmatrix}$	$\begin{bmatrix} \frac{\mathrm{i}k^3}{\zeta_1\varepsilon}\mathrm{p} \\ \frac{\mathrm{i}k^4}{\zeta_2\varepsilon}\mathrm{Q}^{\mathrm{e}} \\ \frac{\mathrm{i}k^5}{\zeta_3\varepsilon}\mathrm{O}^{\mathrm{e}} \\ \frac{-k^2\eta}{\zeta_1}\mathrm{m} \\ \frac{-k^4\eta}{\zeta_2}\mathrm{Q}^{\mathrm{m}} \\ \frac{-k^5\eta}{\zeta_3}\mathrm{O}^{\mathrm{m}} \end{bmatrix} = \begin{bmatrix} \bar{\bar{F}}_1\mathrm{b}^{\mathrm{e}}_1 \\ \bar{\bar{F}}_2\mathrm{b}^{\mathrm{e}}_2 \\ \bar{\bar{F}}_3\mathrm{b}^{\mathrm{e}}_3 \\ \bar{\bar{F}}_1\mathrm{b}^{\mathrm{m}}_1 \\ \bar{\bar{F}}_2\mathrm{b}^{\mathrm{m}}_2 \\ \bar{\bar{F}}_3\mathrm{b}^{\mathrm{m}}_3 \end{bmatrix}$	$\begin{bmatrix} \zeta_1^{-1}\varepsilon^{-1}\mathrm{p} \\ \frac{k}{\zeta_2\varepsilon}\mathrm{Q}^{\mathrm{e}} \\ \frac{k^2}{\zeta_3\varepsilon}\mathrm{O}^{\mathrm{e}} \\ \frac{\mathrm{i}\eta}{\zeta_1}\mathrm{m} \\ \frac{\mathrm{i}k\eta}{\zeta_2}\mathrm{Q}^{\mathrm{m}} \\ \frac{\mathrm{i}k^2\eta}{\zeta_3}\mathrm{O}^{\mathrm{m}} \end{bmatrix} = \frac{\bar{\bar{\tilde{\alpha}}}}{k^3} \begin{bmatrix} \zeta_1\mathrm{E}_1 \\ \frac{\zeta_2}{k}\mathrm{E}_2 \\ \frac{\zeta_3}{k^2}\mathrm{E}_3 \\ \mathrm{i}\eta\zeta_1\mathrm{H}_1 \\ \frac{\mathrm{i}\eta\zeta_2}{k}\mathrm{H}_2 \\ \frac{\mathrm{i}\eta\zeta_3}{k^2}\mathrm{H}_3 \end{bmatrix}$
$\bar{\bar{T}}_0 = \begin{bmatrix} \bar{\bar{T}}^{\mathrm{ee}} & \bar{\bar{T}}^{\mathrm{em}} \\ \bar{\bar{T}}^{\mathrm{me}} & \bar{\bar{T}}^{\mathrm{mm}} \end{bmatrix}$	$\bar{\bar{\tilde{\alpha}}}^{\nu\nu'}_{jj'} = -\mathrm{i}\bar{\bar{F}}_j \bar{\bar{T}}^{\nu\nu'}_{jj'} \bar{\bar{F}}_{j'}^{-1}$	$\bar{\bar{\tilde{\alpha}}}_0 = \begin{bmatrix} \bar{\bar{\tilde{\alpha}}}^{\mathrm{ee}} & \bar{\bar{\tilde{\alpha}}}^{\mathrm{em}} \\ \bar{\bar{\tilde{\alpha}}}^{\mathrm{me}} & \bar{\bar{\tilde{\alpha}}}^{\mathrm{mm}} \end{bmatrix}$
$\bar{\bar{T}}_{\mathrm{eff}} = (\bar{\bar{I}} - \bar{\bar{T}}_0\bar{\bar{C}}_{\mathrm{s}})^{-1}\bar{\bar{T}}_0$	$\bar{\bar{C}} = \mathrm{i}\bar{\bar{F}}\bar{\bar{C}}_{\mathrm{s}}\bar{\bar{F}}^{-1}$	$\bar{\bar{\tilde{\alpha}}}_{\mathrm{eff}} = (\bar{\bar{I}} - \bar{\bar{\tilde{\alpha}}}_0\bar{\bar{C}})^{-1}\bar{\bar{\tilde{\alpha}}}_0$

a) $\Gamma = \frac{\mathrm{i}\sqrt{\pi}\,\mathrm{e}^{\mathrm{i}\mathbf{k}^{\pm}_{\mathrm{G}}\cdot\mathbf{r}}}{2Ak^2\,|\cos\theta|}$, $A = \Lambda_1\Lambda_2$, $\mathbf{k}^{\pm}_{\mathrm{G}} = \mathbf{k}_{\parallel} + \mathbf{G} \pm \hat{\mathbf{z}}\sqrt{k^2 - |\mathbf{k}_{\parallel} + \mathbf{G}|^2}$, $\mathbf{G} = \frac{2\pi n_1}{\Lambda_1}\hat{\mathbf{x}} + \frac{2\pi n_2}{\Lambda_1}\hat{\mathbf{y}}$, $\zeta_j = \sqrt{(2j+1)!\pi}$.

$i = \{1, 2, 3\}$, then the eigenvalue problem can be formulated in spherical coordinates as

$$\left|\bar{\bar{I}} - \bar{\bar{T}}_0\,\bar{\bar{C}}_s\right| = 0 \tag{12}$$

The solutions of Equation (12) are associated with eigenmodes of the metasurface and can be of great importance for research into phenomena related to guided modes or bound states in the continuum. Equivalently, if the Cartesian basis is employed with Equations (2) and (9), then the eigenvalue problem is formulated as

$$\left|\bar{\bar{I}} - \bar{\bar{\tilde{\alpha}}}_0\,\bar{\bar{C}}\right| = 0 \tag{13}$$

which was solved in ref. [96] for the case of 2D arrays of electric and magnetic dipoles.

Once the response of the metasurface is calculated, the contribution of substrates can, in general, be calculated using the layer method, as explained in ref. [69]. Specifically, one can get the total response by successfully coupling the interfaces and the media involved in the whole structure. The calculation of the scattering response of the metasurface is here the most crucial and challenging part. Nevertheless, properly treating particle arrays on metasurfaces is not a trivial matter; generally, the T matrix representation of a particle is valid only outside the smallest sphere that includes the particle (this is the "Rayleigh Hypothesis"), and, thus, the output may diverge, when substrate interfaces are placed inside this sphere. The T or polarizability matrix method could still produce accurate results, though, provided that a sufficient and correct multipolar expansion order that includes evanescent modes and more diffraction orders are used.[69,97] In this work, where only the propagating modes are calculated in Equation (4) or (7), the employment of the layer method[69] to include the substrate effects can usually be only an approximation and, thus, not shown herein. However, this approximate solution could, in some cases, shed light on interesting optical phenomena, such as collective resonances in metasurfaces affected by a nonhomogenous environment.[38]

Let us, now, assume specific symmetries about the geometry of the particles in use or a particular wave incidence onto the metasurface. In that case, the closed-form equations provided in this section can be further simplified to accessible analytical formulas that could greatly assist the metasurface design process. This approach will be demonstrated in the following sections. The next section is dedicated to normal incidence, while the next but one section is dedicated to oblique incidence.

3. Analytic Equations: Normal Incidence

3.1. Propagating Diffraction Orders of Dipole-Quadrupole Metasurfaces Made from Isotropic Meta-Atoms

In this subsection, originating from Equation (11), we derive a general, simplified, closed-form, analytic expression for the amplitudes of the propagating diffraction orders from dipole–quadrupole metasurfaces and metagratings made from isotropic meta-atoms and illuminated at normal incidence. An isotropic particle has spherical symmetry and includes homogeneous/core-multishell spheres and isotropic colloidal particles.[98] Unlike previous modeling efforts, our analytic procedure captures the amplitudes in reflection and transmission of the zeroth diffraction orders, as well as higher propagating diffraction ones.

The analytical formulas, in this work, are developed on the spherical basis and presented on the Cartesian basis. The two bases are equivalent and interchangeable. While the Cartesian basis is more popular in the metasurface community and provides more intuitive understanding for lower-order multipolar orders, the spherical basis, enables an accurate description of the particle scattering and coupling. By employing the vector spherical harmonics, it is possible to compute the lattice coupling matrix quickly, thus, calculating the interaction between particles on the 2D array under study accurately and without approximations, unlike other attempts that employ the Cartesian basis (Section S.I.C, Supporting Information). For the general case, we provide the formulas for the response of a metasurface both for the Cartesian and the spherical basis, as presented in Table 1. We leave the choice to the user according to the specific problem under study.

For isolated isotropic particles, as shown in Figure 2f, the polarizability matrix is diagonal. Thus, the elements of the matrix $\overline{\overline{\tilde{\alpha}}}_0$ can be written via Equation (2) as

$$\overline{\overline{\tilde{\alpha}}}^{\mathrm{ee}}_{11} = \tilde{\alpha}_{\mathrm{p}}\overline{\overline{I}}, \quad \overline{\overline{\tilde{\alpha}}}^{\mathrm{mm}}_{11} = \tilde{\alpha}_{\mathrm{m}}\overline{\overline{I}} \tag{14a}$$

$$\overline{\overline{\tilde{\alpha}}}^{\mathrm{ee}}_{22} = \tilde{\alpha}_{\mathrm{Q^e}}\overline{\overline{I}}, \quad \overline{\overline{\tilde{\alpha}}}^{\mathrm{mm}}_{22} = \tilde{\alpha}_{\mathrm{Q^m}}\overline{\overline{I}} \tag{14b}$$

where $\tilde{\alpha}_{\mathrm{p}}$ ($\tilde{\alpha}_{\mathrm{m}}$), and $\tilde{\alpha}_{\mathrm{Q^e}}$ ($\tilde{\alpha}_{\mathrm{Q^m}}$) are the normalized electric (magnetic) dipole and quadrupole polarizabilities, respectively. The dimensions of the unitary matrix, $\overline{\overline{I}}$, changes according to the multipolar order, that is, 3 × 3 for dipole and 5 × 5 for quadrupole. These polarizabilities can be linked to the Mie coefficients via Equation (3), as[16,60]

$$\tilde{\alpha}_{\mathrm{p}} = \mathrm{i}a_1, \quad \tilde{\alpha}_{\mathrm{m}} = \mathrm{i}b_1 \tag{15a}$$

$$\tilde{\alpha}_{\mathrm{Q^e}} = \mathrm{i}a_2, \quad \tilde{\alpha}_{\mathrm{Q^m}} = \mathrm{i}b_2 \tag{15b}$$

where a_j (b_j) is the electric (magnetic) Mie coefficient of j's order. When inside the lattice, these polarizabilities will be modulated and coupled to each other according to Equation (9).

For normal incidence, or $\theta_{\mathrm{inc}} = 0$, the incident TE and TM polarizations can be defined as

$$\mathbf{E}^{\mathrm{inc}}_{\mathrm{TM}} = \begin{bmatrix} E_x \\ E_y \\ E_z \end{bmatrix} = E_0 \begin{bmatrix} 1 \\ 0 \\ 0 \end{bmatrix} \mathrm{e}^{\mathrm{i}kz} \tag{16a}$$

$$\mathbf{E}^{\mathrm{inc}}_{\mathrm{TE}} = \begin{bmatrix} E_x \\ E_y \\ E_z \end{bmatrix} = E_0 \begin{bmatrix} 0 \\ 1 \\ 0 \end{bmatrix} \mathrm{e}^{\mathrm{i}kz} \tag{16b}$$

In this work, TE/TM polarizations are equivalent to s-/p-polarizations, where the E-field vector direction is the same as the unit-vectors of the spherical coordinates' system, $\hat{\phi}$ and $\hat{\theta}$, respectively (Sections S.I.A and S.I.B, Supporting Information).

Let us now consider the calculation of the lattice coupling matrix. For a square array and under normal incidence, $\overline{\overline{C}}$ has a simpler symmetry with many symmetry-protected zeros. Additionally, for isotropic particles with elements described in Equation (14), not all coupling coefficients enter Equation (11), further simplifying calculations. In **Figure 3**a, we show the Cartesian coupling matrix under normal incidence for an exemplary normalized periodicity of $\tilde{\Lambda} = 0.9$ up to quadrupolar order and the relevant elements of $\overline{\overline{C}}$ for isotropic constituents are marked. In Figure 3b,c, the real and imaginary parts of the relevant coupling coefficients are shown versus the normalized lattice periodicity. The relevant lattice coefficients for the specific normal incidence and square lattice calculations are dipole–dipole C_{dd}, quadrupole–quadrupole C_{QQ}, and dipole–quadrupole C_{dQ} couplings. As their name suggests, they are coefficients for the coupling of multipoles of a different order. The imaginary parts of these coefficients can be analytically calculated using energy conservation relations. We have calculated, herein, the imaginary part of these coefficients for subwavelength metasurfaces using the analytic equations for transmission and reflection (Section S.VII, Supporting Information) as

$$\Im(C_{\mathrm{dd}}) = \frac{3}{4\pi\tilde{\Lambda}^2} - 1 \tag{17a}$$

$$\Im(C_{\mathrm{QQ}}) = \frac{5}{4\pi\tilde{\Lambda}^2} - 1 \tag{17b}$$

$$\Im(C_{\mathrm{dQ}}) = \frac{\sqrt{15}}{4\pi\tilde{\Lambda}^2} \tag{17c}$$

The imaginary parts above can be used to determine fundamental limits. The imaginary part of the dipole–dipole lattice coupling has already been identified in the literature.[37]

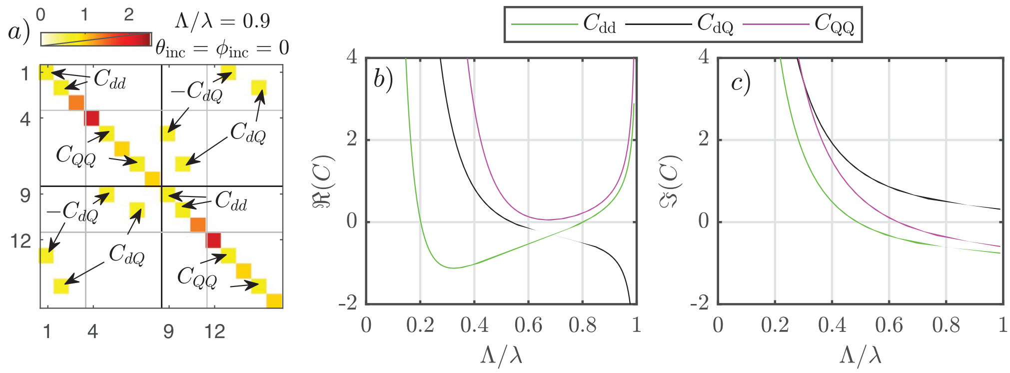

Figure 3. The Cartesian coupling matrix: a) The Cartesian coupling matrix amplitude for a square array with a normalized periodicity of $\Lambda/\lambda = 0.9$ under normal incidence ($\theta_{\mathrm{inc}} = \phi_{\mathrm{inc}} = 0$) up to quadrupolar order. The relevant matrix elements for a metasurface made from isotropic particles are dipole–dipole C_{dd}, quadrupole–quadrupole C_{QQ}, and dipole–quadrupole C_{dQ} couplings. They are marked with an arrow. b) The real and c) imaginary part of the relevant lattice couplings as a function of the normalized periodicity Λ/λ. For a square array, the electric and magnetic parts are equal.

The real part of the coupling coefficients (Figure 3b) cannot be analytically derived, and infinite summations, as discussed before, are required for accurate calculations. The real part of the coupling coefficients can be linked to the detuning of the response of the isolated meta-atoms.[99,100]

In the next step, we calculate the effective multipole moments induced in each particle in the lattice as a function of the effective Mie coefficients up to quadrupolar order for both TM and TE polarized excitation. For TM incidence, they are analytically expressed as

$$\begin{bmatrix} p_x/\varepsilon \\ Q^{\mathrm{e}}_{\mathrm{xz}}/\varepsilon \\ \eta m_y \\ \eta Q^{\mathrm{m}}_{\mathrm{yz}} \end{bmatrix} = \begin{bmatrix} \frac{6\pi \mathrm{i}}{k^3} a_{1,\mathrm{mod}}^{b_2} \\ \frac{-60\pi}{k^4} a_{2,\mathrm{mod}}^{b_1} \\ \frac{6\pi \mathrm{i}}{k^3} b_{1,\mathrm{mod}}^{a_2} \\ \frac{-60\pi}{k^4} b_{2,\mathrm{mod}}^{a_1} \end{bmatrix} E_0 \tag{18a}$$

and for a TE polarized incidence

$$\begin{bmatrix} p_y/\varepsilon \\ Q^{\mathrm{e}}_{\mathrm{yz}}/\varepsilon \\ \eta m_x \\ \eta Q^{\mathrm{m}}_{\mathrm{xz}} \end{bmatrix} = \begin{bmatrix} \frac{6\pi \mathrm{i}}{k^3} a_{1,\mathrm{mod}}^{b_2} \\ \frac{-60\pi}{k^4} a_{2,\mathrm{mod}}^{b_1} \\ \frac{-6\pi \mathrm{i}}{k^3} b_{1,\mathrm{mod}}^{a_2} \\ \frac{60\pi}{k^4} b_{2,\mathrm{mod}}^{a_1} \end{bmatrix} E_0 \tag{18b}$$

The effective Mie coefficients/polarizabilities of the particles in these expressions above depend on a) the modulation of the elements of the same multipolar order through C_{dd} and C_{QQ} and b) the coupling with other multipole moments in the lattice through C_{dQ}. The b_2 superscript shows the coupled parameters, and the coupling term is written in the circle. Electric (magnetic) dipole moments are coupled to magnetic (electric) quadrupole moments and vice versa. The modulated and coupled Mie coefficients, that are commonly called the effective Mie coefficients, can be written as

$$\frac{1}{a_{1,\mathrm{eff}}} = \frac{1}{a_{1,\mathrm{mod}}^{b_2}} = \frac{1 + C_{\mathrm{dQ}}^2 b_{2,\mathrm{mod}} a_{1,\mathrm{mod}}}{a_{1,\mathrm{mod}}\left(1 + \mathrm{i}\sqrt{5/3}\, C_{\mathrm{dQ}} b_{2,\mathrm{mod}}\right)} \tag{19a}$$

$$\frac{1}{b_{1,\mathrm{eff}}} = \frac{1}{b_{1,\mathrm{mod}}^{a_2}} = \frac{1 + C_{\mathrm{dQ}}^2 a_{2,\mathrm{mod}} b_{1,\mathrm{mod}}}{b_{1,\mathrm{mod}}\left(1 + \mathrm{i}\sqrt{5/3}\, C_{\mathrm{dQ}} a_{2,\mathrm{mod}}\right)} \tag{19b}$$

$$\frac{1}{a_{2,\mathrm{eff}}} = \frac{1}{a_{2,\mathrm{mod}}^{b_1}} = \frac{1 + C_{\mathrm{dQ}}^2 b_{1,\mathrm{mod}} a_{2,\mathrm{mod}}}{a_{2,\mathrm{mod}}\left(1 + \mathrm{i}\sqrt{3/5}\, C_{\mathrm{dQ}} b_{1,\mathrm{mod}}\right)} \tag{19c}$$

$$\frac{1}{b_{2,\mathrm{eff}}} = \frac{1}{b_{2,\mathrm{mod}}^{a_1}} = \frac{1 + C_{\mathrm{dQ}}^2 a_{1,\mathrm{mod}} b_{2,\mathrm{mod}}}{b_{2,\mathrm{mod}}\left(1 + \mathrm{i}\sqrt{3/5}\, C_{\mathrm{dQ}} a_{1,\mathrm{mod}}\right)} \tag{19d}$$

The modulated Mie coefficients in Equation (19) are explicitly written as

$$\frac{1}{a_{1,\mathrm{mod}}} = \frac{1}{a_1} - \mathrm{i}C_{\mathrm{dd}}, \quad \frac{1}{b_{1,\mathrm{mod}}} = \frac{1}{b_1} - \mathrm{i}C_{\mathrm{dd}} \tag{20a}$$

$$\frac{1}{a_{2,\mathrm{mod}}} = \frac{1}{a_2} - \mathrm{i}C_{\mathrm{QQ}}, \quad \frac{1}{b_{2,\mathrm{mod}}} = \frac{1}{b_2} - \mathrm{i}C_{\mathrm{QQ}} \tag{20b}$$

Writing the above expression in such a manner has the immediate advantage of distinguishing the effect of the lattice and the single meta-atom response on the effective response. It is worth mentioning that despite a different approach, the above equations are very similar to the equations in ref. [67]. In ref. [101], we have exploited the effective moments in Equations (18a,b) to find operation regimes in which the magnetic dipole moment can be colossally enhanced.

By calculating the relevant lattice coupling matrix elements and polarizabilities of the isolated, isotropic particle and by deriving the effective Mie coefficients with Equation (19), the general equation for square lattices (11), can be simplified for both polarizations to

$$\begin{bmatrix} E^{\mathrm{sca}}_{\mathrm{TE}_{0,0}\to\mathrm{TE}_{n1,n2}} & E^{\mathrm{sca}}_{\mathrm{TE}_{0,0}\to\mathrm{TM}_{n1,n2}} \\ E^{sca}_{TM_{0,0}\to TE_{n1,n2}} & E^{\mathrm{sca}}_{\mathrm{TM}_{0,0}\to\mathrm{TM}_{n1,n2}} \end{bmatrix} = -\frac{\cos\phi\,\mathrm{sgn}(\cos\theta)}{4\pi\tilde{\Lambda}^2}\times$$

$$\begin{bmatrix} \left(\dfrac{3a_{1,\mathrm{eff}}}{\cos\theta}+3b_{1,\mathrm{eff}}+5a_{2,\mathrm{eff}}+\dfrac{5\cos 2\theta b_{2,\mathrm{eff}}}{\cos\theta}\right) & \left(3a_{1,\mathrm{eff}}+\dfrac{3b_{1,\mathrm{eff}}}{\cos\theta}+\dfrac{5\cos 2\theta a_{2,\mathrm{eff}}}{\cos\theta}+5b_{2,\mathrm{eff}}\right)\tan\phi \\ -\left(\dfrac{3a_{1,\mathrm{eff}}}{\cos\theta}+3b_{1,\mathrm{eff}}+5a_{2,\mathrm{eff}}+\dfrac{5\cos 2\theta b_{2,\mathrm{eff}}}{\cos\theta}\right)\tan\phi & \left(3a_{1,\mathrm{eff}}+\dfrac{3b_{1,\mathrm{eff}}}{\cos\theta}+\dfrac{5\cos 2\theta a_{2,\mathrm{eff}}}{\cos\theta}+5b_{2,\mathrm{eff}}\right) \end{bmatrix} \tag{21}$$

with

$$\theta=\arccos\left[\pm\sqrt{1-\frac{1}{\tilde{\Lambda}^2}(n_1^2+n_2^2)}\right] \tag{22a}$$

$$\phi=\arctan\left(\frac{n_2}{n_1}\right) \tag{22b}$$

where (n_1, n_2) label the different diffraction orders. Note that the modes are propagating if θ is real. For $\theta > \pi/2$, that is, scattering in the backward half-sphere, $\cos\theta$ is negative. Hence, using Equation (21), the transmission and reflection through a dipolar–quadrupolar metasurface with isotropic constituents can be calculated. The derived formulas from this subsection are conveniently summarized in **Table 2**A.

3.2. Zeroth-Order Transmission and Reflection

Under normal incidence ($\theta_{\mathrm{inc}} = \phi_{\mathrm{inc}} = 0$), if only the zeroth-order mode is considered, or, simply, a nondiffracting square

Table 2. Reflection and transmission coefficients for metasurfaces under A) normal and B) oblique incidence. A.1,B.1) Effective Mie coefficients (coupled and modulated). A.2,B.2) Modulated Mie coefficients. A.3) General equations.

A) Normal incidence*: $\theta_{\mathrm{inc}}=\phi_{\mathrm{inc}}=0$	
	$\begin{bmatrix} \{t,r\}_{\mathrm{TE}_{0,0}\to\mathrm{TE}_{n_1,n_2}} & \{t,r\}_{\mathrm{TE}_{0,0}\to\mathrm{TM}_{n_1,n_2}} \\ \{t,r\}_{\mathrm{TM}_{0,0}\to\mathrm{TE}_{n_1,n_2}} & \{t,r\}_{\mathrm{TM}_{0,0}\to\mathrm{TM}_{n_1,n_2}} \end{bmatrix} = \frac{1\pm 1}{2}\begin{bmatrix} \delta_{n_1n_20} & 0 \\ 0 & \delta_{n_1n_20}\end{bmatrix} - \frac{\pm\cos\phi}{4\pi\tilde{\Lambda}^2}\times \begin{bmatrix} \left(\frac{3a_{1,\mathrm{eff}}}{\cos\theta}+3b_{1,\mathrm{eff}}+5a_{2,\mathrm{eff}}+\frac{5\cos 2\theta b_{2,\mathrm{eff}}}{\cos\theta}\right) & \left(3a_{1,\mathrm{eff}}+\frac{3b_{1,\mathrm{eff}}}{\cos\theta}+\frac{5\cos 2\theta a_{2,\mathrm{eff}}}{\cos\theta}+5b_{2,\mathrm{eff}}\right)\tan\phi \\ -\left(\frac{3a_{1,\mathrm{eff}}}{\cos\theta}+3b_{1,\mathrm{eff}}+5a_{2,\mathrm{eff}}+\frac{5\cos 2\theta b_{2,\mathrm{eff}}}{\cos\theta}\right)\tan\phi & \left(3a_{1,\mathrm{eff}}+\frac{3b_{1,\mathrm{eff}}}{\cos\theta}+\frac{5\cos 2\theta a_{2,\mathrm{eff}}}{\cos\theta}+5b_{2,\mathrm{eff}}\right) \end{bmatrix}$
A.1	$\frac{1}{a_{1,\mathrm{eff}}}=\frac{1+C_{\mathrm{dQ}}^2 b_{2,\mathrm{mod}}a_{1,\mathrm{mod}}}{a_{1,\mathrm{mod}}(1+\mathrm{i}\sqrt{5/3}C_{\mathrm{dQ}}b_{2,\mathrm{mod}})},\ \frac{1}{b_{1,\mathrm{eff}}}=\frac{1+C_{\mathrm{dQ}}^2 a_{2,\mathrm{mod}}b_{1,\mathrm{mod}}}{b_{1,\mathrm{mod}}(1+\mathrm{i}\sqrt{5/3}C_{\mathrm{dQ}}a_{2,\mathrm{mod}})},\ \frac{1}{a_{2,\mathrm{eff}}}=\frac{1+C_{\mathrm{dQ}}^2 b_{1,\mathrm{mod}}a_{2,\mathrm{mod}}}{a_{2,\mathrm{mod}}(1+\mathrm{i}\sqrt{3/5}C_{\mathrm{dQ}}b_{1,\mathrm{mod}})},\ \frac{1}{b_{2,\mathrm{eff}}}=\frac{1+C_{\mathrm{dQ}}^2 a_{1,\mathrm{mod}}b_{2,\mathrm{mod}}}{b_{2,\mathrm{mod}}(1+\mathrm{i}\sqrt{3/5}C_{\mathrm{dQ}}a_{1,\mathrm{mod}})}$
A.2	$\frac{1}{a_{1,\mathrm{mod}}}=\frac{1}{a_1}-\mathrm{i}C_{\mathrm{dd}},\ \frac{1}{b_{1,\mathrm{mod}}}=\frac{1}{b_1}-\mathrm{i}C_{\mathrm{dd}},\ \frac{1}{a_{2,\mathrm{mod}}}=\frac{1}{a_2}-\mathrm{i}C_{\mathrm{QQ}},\ \frac{1}{b_{2,\mathrm{mod}}}=\frac{1}{b_2}-\mathrm{i}C_{\mathrm{QQ}}$
A.3	$\theta=\arccos\left[\pm\sqrt{1-\frac{1}{\tilde{\Lambda}^2}(n_1^2+n_2^2)}\right],\quad \phi=\arctan\left(\frac{n_2}{n_1}\right),\quad \tilde{\Lambda}=\frac{\Lambda}{\lambda}$
B) Oblique incidence: $\phi_{\mathrm{inc}}=0$	
	$\begin{bmatrix} t_{\mathrm{TE}_{0,0}\to\mathrm{TE}_{0,0}} \\ t_{\mathrm{TM}_{0,0}\to\mathrm{TM}_{0,0}} \end{bmatrix} = \begin{bmatrix} 1 \\ 1 \end{bmatrix} - \frac{3}{4\pi\tilde{\Lambda}^2\lvert\cos\theta_{\mathrm{inc}}\rvert}\begin{bmatrix} b_{1,\mathrm{mod.xx}}\cos^2\theta_{\mathrm{inc}}+a_{1,\mathrm{eff.yy}}+b_{1,\mathrm{eff.zz}}\sin^2\theta_{\mathrm{inc}} \\ a_{1,\mathrm{mod.xx}}\cos^2\theta_{\mathrm{inc}}+b_{1,\mathrm{eff.yy}}+a_{1,\mathrm{eff.zz}}\sin^2\theta_{\mathrm{inc}} \end{bmatrix}$
	$\begin{bmatrix} r_{\mathrm{TE}_{0,0}\to\mathrm{TE}_{0,0}} \\ r_{\mathrm{TM}_{0,0}\to\mathrm{TM}_{0,0}} \end{bmatrix} = \frac{3}{4\pi\tilde{\Lambda}^2\lvert\cos\theta_{\mathrm{inc}}\rvert}\begin{bmatrix} b_{1,\mathrm{mod.xx}}\cos^2\theta_{\mathrm{inc}}-a_{1,\mathrm{eff.yy}}-b_{1,\mathrm{eff.zz}}\sin^2\theta_{\mathrm{inc}} \\ a_{1,\mathrm{mod.xx}}\cos^2\theta_{\mathrm{inc}}-b_{1,\mathrm{eff.yy}}-a_{1,\mathrm{eff.zz}}\sin^2\theta_{\mathrm{inc}} \end{bmatrix}$
B.1	$\frac{1}{a_{1,\mathrm{eff.yy}}}=\frac{1-C_{\mathrm{yz}}^2 b_{1,\mathrm{mod.zz}}a_{1,\mathrm{mod.yy}}}{a_{1,\mathrm{mod.yy}}(1-C_{\mathrm{yz}}b_{1,\mathrm{mod.zz}}\sin\theta_{\mathrm{inc}})},\ \frac{1}{b_{1,\mathrm{eff.yy}}}=\frac{1-C_{\mathrm{yz}}^2 b_{1,\mathrm{mod.yy}}a_{1,\mathrm{eff.zz}}}{b_{1,\mathrm{mod.yy}}(1-C_{\mathrm{yz}}a_{1,\mathrm{mod.zz}}\sin\theta_{\mathrm{inc}})},\ \frac{1}{a_{1,\mathrm{eff.zz}}}=\frac{1-C_{\mathrm{yz}}^2 b_{1,\mathrm{mod.yy}}a_{1,\mathrm{mod.zz}}}{a_{1,\mathrm{mod.zz}}(1-C_{\mathrm{yz}}b_{1,\mathrm{mod.yy}}\csc\theta_{\mathrm{inc}})},\ \frac{1}{b_{1,\mathrm{eff.zz}}}=\frac{1-C_{\mathrm{yz}}^2 b_{1,\mathrm{mod.zz}}a_{1,\mathrm{mod.yy}}}{b_{1,\mathrm{mod.zz}}(1-C_{\mathrm{yz}}a_{1,\mathrm{mod.yy}}\csc\theta_{\mathrm{inc}})}$
B.2	$\frac{1}{b_{1,\mathrm{mod.xx}}}=\frac{1}{b_1}-\mathrm{i}C_{\mathrm{xx}},\quad \frac{1}{b_{1,\mathrm{mod.zz}}}=\frac{1}{b_1}-\mathrm{i}C_{\mathrm{zz}},\quad \frac{1}{b_{1,\mathrm{mod.yy}}}=\frac{1}{b_1}-\mathrm{i}C_{\mathrm{yy}},\ \frac{1}{a_{1,\mathrm{mod.xx}}}=\frac{1}{a_1}-\mathrm{i}C_{\mathrm{xx}},\quad \frac{1}{a_{1,\mathrm{mod.yy}}}=\frac{1}{a_1}-\mathrm{i}C_{\mathrm{yy}},\quad \frac{1}{a_{1,\mathrm{mod.zz}}}=\frac{1}{a_1}-\mathrm{i}C_{\mathrm{zz}}$

*Note that θ and ϕ are the angles of the scattering field (i.e., for the reflection $\cos\theta < 0$). In A) for '±' use '+' for transmission and '–' for reflection. In B) $k_y^{\mathrm{inc}}=0$.

array with $\Lambda < \lambda$, then the calculation formulas for the reflection ($\theta = \pi$, $\phi = 0$) and transmission ($\theta = \phi = 0$) coefficients for TE/TM polarization can be simplified to

$$t_{\mathrm{TM}} = 1 - \frac{3a_{1,\mathrm{mod}}^{b_2} + 3b_{1,\mathrm{mod}}^{a_2} + 5a_{2,\mathrm{mod}}^{b_1} + 5b_{2,\mathrm{mod}}^{a_1}}{4\pi\widetilde{\Lambda}^2} \tag{23a}$$

$$r_{\mathrm{TM}} = \frac{3a_{1,\mathrm{mod}}^{b_2} - 3b_{1,\mathrm{mod}}^{a_2} - 5a_{2,\mathrm{mod}}^{b_1} + 5b_{2,\mathrm{mod}}^{a_1}}{4\pi\widetilde{\Lambda}^2} \tag{23b}$$

$$t_{\mathrm{TE}} = t_{\mathrm{TM}} \tag{23c}$$

$$r_{\mathrm{TE}} = -r_{\mathrm{TM}} \tag{23d}$$

Note that the reflection phase for the TE and TM polarizations are the same, and the sign difference is only due to the specific definition of the TE and TM vectors. The final equations above, for this specific case of a square lattice, normal incidence, and isotropic consisting particles are very similar to the equations derived by ref. [102].

3.3. Bound States in the Continuum

As discussed in Section 2, the expression for the effective T or polarizability matrix can provide the formulation of the general-case eigenvalue problem, as demonstrated in Equations (12) and (13). Solving these equations, either on the Cartesian or spherical basis, one can obtain the modes propagating or bound on the metasurface. In this subsection, we will demonstrate how bound states in the continuum (BICs) on metasurfaces[1,39,96] can be identified and possibly engineered using the analytical formulas presented in Section 3.1.

Let us now form the eigenvalue problem of Equation (13), for the reduced case of a 2D array of identical isotropic particles with an induced electric dipole and a magnetic quadrupole, and under normal incidence. Starting from Equation (18a) for the TM incidence, we remove the magnetic dipole and the electric quadrupole and, eventually, we write the analytical formulas in a matrix form. In the absence of excitation, in order for the system to have a nontrivial solution, the determinant of the inverse effective polarizability matrix must be zero. After some algebra, the condition for the modes of the metasurface is reached (Section S.X, Supporting Information), as

$$1 + C_{\mathrm{dQ}}^2\, a_{1,\mathrm{mod}}\, b_{2,\mathrm{mod}} = 0 \tag{24}$$

The same condition can be reached for the TE incidence due to symmetry. Because normal incidence is enforced in Equation (18a), no propagating modes on the metasurface exist. Thus, the solutions of Equation (24) correspond to the BICs of the 2D array.

This derived condition above for identifying BICs can, afterward, be utilized for engineering 2D arrays with bound states and, most important, quasi-BICs with very high Q-factor. If the Mie coefficient a_1 is kept constant, the b_2 coefficients that satisfy the condition Equation (24) are

$$b_2 = \frac{1 - \mathrm{i}a_1 C_{\mathrm{dd}}}{a_1\left(C_{\mathrm{dd}} C_{\mathrm{QQ}} - C_{\mathrm{dQ}}^2\right) + \mathrm{i}C_{\mathrm{QQ}}} \tag{25a}$$

with

$$\Re\{b_2\} = |b_2|^2 \tag{25b}$$

The condition (25b) is necessary to obtain physically meaningful solutions from Equation (25a), that correspond to realistic and non-absorbing scatterers.

Let us now explore an example to demonstrate how Equation (25) can predict the location of a BIC. For this purpose, we will employ the Mie angles representation of Mie coefficients[103], that is, θ_{E1} and θ_{M2} for a_1 and b_2, respectively (Appendix H). If we arbitrarily choose an electric dipole with the Mie coefficient $a_1 = 1$ (or $\theta_{\mathrm{E1}} = 0$), then, the only solution at a normalized periodicity interval $\Lambda/\lambda = [0.1, 1]$ from (25) is $b_2 = 0.7855 - \mathrm{i}0.4105$ (or $\theta_{\mathrm{M2}} = -0.4815$ rad) and at $\Lambda/\lambda = 0.7114$.

In the next step, we calculate the transmission from the same 2D array for $\theta_{\mathrm{E1}} = 0$ and for sweeping through all the Mie angles θ_{M2} via Equation (21). The results are depicted in **Figure 4**a. As shown, for $\theta_{\mathrm{M2}} = -0.4815$ and $\Lambda/\lambda = 0.7114$, the $|t| = 0$ or $|t| = 1$ resonances are nullified, demonstrating that Equation (24) provide the BIC's wavelength location, as well as the θ_{E1} and θ_{M2} combinations required. Finally, knowing the parameters for engineering a BIC, one can easily, afterward, construct a high-Q quasi-BIC resonance, that interacts with the environment. In Figure 4b, it is demonstrated that, if a slight deviation from the θ_{M2} that fulfills Equation (25) is imposed, then a very sharp quasi-BIC resonance is produced. Eventually, particle swarm optimization method[104] can be employed to design core–shell spheres with the corresponding θ_{E1} and θ_{M2}, to realize the proposed setup.[101]

3.4. Single Multipolar Resonance

This subsection explores metasurfaces made from isotropic particles that only support a single multipolar resonance while other multipolar components are negligible. In such exploration, the effective Mie coefficients in Equation (19) are simplified and are equal to the modulated Mie coefficients in Equation (20). The investigation helps identify the contribution of a single multipolar order in the collective response of the lattice.

3.4.1. Collective Lattice Resonances

The collective lattice resonance (CLR) refers to the resonance in the collective response of the infinitely periodic arrangement of the identical particles.[105,106] Using the derived analytical equations, we can explore how the resonance spectrum of an isolated particle changes collectively inside the infinite lattice. If we assume a square lattice decorated with identical isotropic particles supporting only a single magnetic dipole resonance and vanishing higher-order moments, from Equation (23) the zeroth-order transmission and reflection of the metasurface under normal incidence simplifies to

$$t_{\mathrm{TE}} = 1 + r_{\mathrm{TE}} = 1 - \frac{3}{4\pi\tilde{\Lambda}^2}\left(\frac{1}{1/b_1 - \mathrm{i}C_{\mathrm{dd}}}\right) \tag{26}$$

For a metasurface made from particles supporting a single resonance, at the collective lattice resonance, the transmission drops to zero and all the light is reflected. Therefore, to derive the condition for the lattice resonance, we need to solve the following equation

$$\frac{3}{4\pi\tilde{\Lambda}^2}\left(\frac{1}{1/b_1 - \mathrm{i}C_{\mathrm{dd}}}\right) = 1 \tag{27}$$

To solve the above equation, we exploit the Mie angles to represent any possible Mie coefficients[103] (Appendix H). Here, we only assume nonabsorbing particles represented with a (detuning) magnetic dipole Mie angle θ_{M1}. Inserting the imaginary part of the coupling coefficient from Equation (17) and using the Mie angle representation, after some algebra, the lattice resonance condition is derived as (Section S.XI, Supporting Information)

$$\tan\theta_{\mathrm{M1}} = -\Re\{C_{\mathrm{dd}}\} \tag{28}$$

The above condition is equivalent to putting the real part of the denominator in Equation (27) to zero. This condition is used in refs. [105, 106] to find the CLR in a dipolar metasurface. For a metasurface made from isotropic particles with other single resonances up to a quadrupolar order, the CLR condition can similarly be derived as

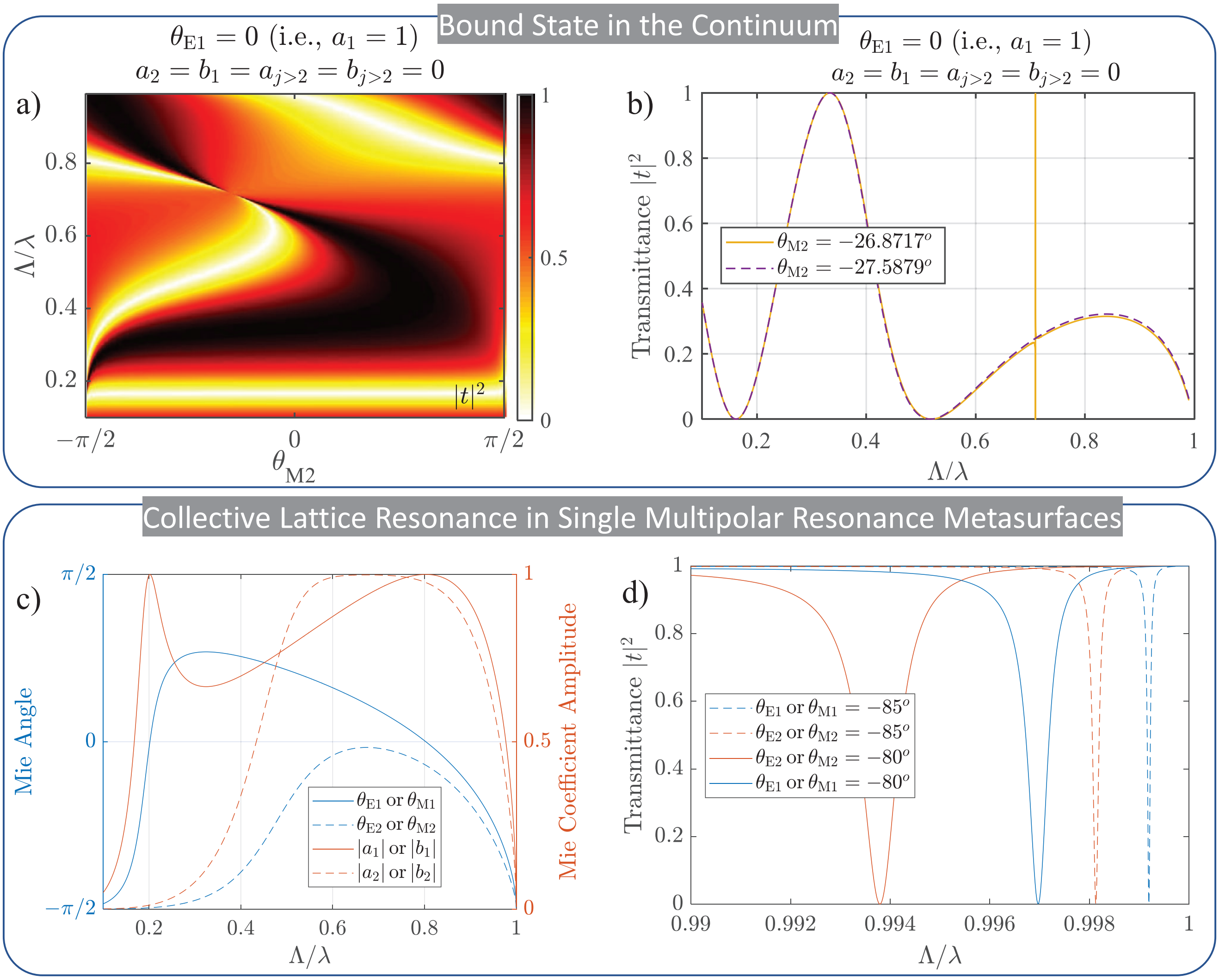

Figure 4. Applications of the analytical formulas for normal incidence: a) The transmittance of a metasurface made from isotropic particles supporting only electric dipole and magnetic quadrupole as a function of the magnetic quadrupole Mie angle θ_{M2} and the normalized periodicity Λ/λ. The electric dipole Mie angle is set to zero, that is, $\theta_{\mathrm{E1}} = 0$, and all other Mie coefficients are assumed negligible. b) The transmittance of the same metasurface as a) for $\theta_{\mathrm{M2}} = -0.4815$ rad (or $\theta_{\mathrm{M2}} = -27.5879°$) and $\theta_{\mathrm{M2}} = -0.469$ rad (or $\theta_{\mathrm{M2}} = -26.8717°$), as a function of the normalized periodicity Λ/λ. Similarly, $\theta_{\mathrm{E1}} = 0$ and all other Mie coefficients are assumed negligible. c) The required Mie angles for the collective lattice resonance (i.e., where $t = 0$), in a single multipolar resonance metasurface illuminated under normal incidence, as a function of the normalized periodicity Λ/λ. The equivalent Mie coefficient amplitude is also shown for simplicity. The plot is based on Equations (28) and (29a). d) The transmittance of a single multipolar resonance metasurface near the point of diffraction. For (c) and (d) the identical particles building the metasurface are isotropic and support a single Mie coefficient, represented by the Mie angle in the legend, while the rest are assumed negligible.

$$\tan\theta_{\mathrm{E1}} = -\Re\{C_{\mathrm{dd}}\} \tag{29a}$$

$$\tan\theta_{\mathrm{M2}} = -\Re\{C_{\mathrm{QQ}}\} \tag{29b}$$

$$\tan\theta_{\mathrm{E2}} = -\Re\{C_{\mathrm{QQ}}\} \tag{29c}$$

where θ_{E1} is the electric dipole Mie angle, and the θ_{M2} (θ_{E2}) is the magnetic (electric) quadrupole Mie angle. Figure 4c shows the required Mie angle that is required for each normalized periodicity in a metasurface supporting a single multipolar resonance for a CLR. The equivalent Mie coefficient amplitude is also shown for simplicity.

For the magnetic dipole metasurface, when the isolated particle is at the resonance (i.e., $b_1 = 1$ or $\theta_{\mathrm{M1}} = 0$), the lattice resonance occurs at normalized periodicities where the real part of the dipole–dipole coupling coefficient vanishes. From Figure 3b, $\Re\{C_{\mathrm{dd}}\}$ crosses zero for two normalized periodicities $\tilde{\Lambda} \approx 0.2, 0.8$ ($\tilde{\Lambda} \approx 0.21, 0.88$ for a Hexagonal lattice). This "magic lattice spacing"[99] is where the "cooperative resonance"[100] of the meta-atoms reflects all the incident light. At this point of operation, the resonance of the isolated meta-atom experiences no detuning, and hence the effective resonance also occurs at the same spacing. The same is true for a metasurface made from particles supporting a single electric dipole moment.

For the quadrupole–quadrupole coupling, $\Re\{C_{\mathrm{QQ}}\}$ does not cross the zero point. Therefore, a spectral detuning between the collective lattice resonance and the quadrupolar resonance of the isolated particle is unavoidable.

From Figure 3b, the large values of the real part of the coupling coefficients for very dense arrangements (i.e., $\Lambda/\lambda \ll 1$) and also subwavelength periodicities close to the wavelength (i.e., $\Lambda/\lambda \approx 1^{-}$) are worth mentioning. For practical reasons, we ignore the dense arrangements in our further analysis. From Equations (28) and (29a), we can find out that for a very large positive real value of the coupling coefficient, the detuning Mie angle required for a lattice resonance tends to an extreme off-resonance case of $-\pi/2$. For an upper value of $\Lambda/\lambda = 1$, the required detuning Mie coefficients are: a_1 or $b_1 = 1.58 \times 10^{-15} - 3.97\mathrm{i} \times 10^{-8}$, a_2 or $b_2 = 5.68 \times 10^{-16} - 2.38\mathrm{i} \times 10^{-8}$. These minuscule Mie coefficients, surprisingly, can rise to a collective resonance of the lattice for the sweet spot periodicity of $\Lambda = \lambda$.

Another interesting feature of near diffraction lattice resonances is the emergence of high Q-factors or sharp features. In Figure 4d, we have plotted the transmission of single resonance metasurface near the point of first diffraction order. It is noted that for very small Mie coefficients, a collective resonance with a very high Q-factor is achievable. The quality factor increases for a weaker Mie coefficient (i.e., larger Mie angle values). Furthermore, as shown in the figure, dipole moments produce sharper resonances as compared to quadrupole moments. Please note, unlike the BIC case that was studied in the previous subsection, the theoretical limit for the quality factor of the resonance is finite.

3.4.2. Optical Cross-Section

It might be interesting to find out the scattering cross-section of a single resonance dipolar meta-atom inside and outside a lattice for the two "magic lattice spacings," that is, at the CLR. In Appendix G, we have calculated the scattering, extinction, and absorption cross-sections in spherical and Cartesian coordinates. For a single magnetic resonance, the scattering cross-section is calculated as

$$\sigma_{\mathrm{sca}}^{\mathrm{c}} = \frac{k^4\eta^2}{|E_0|^2 6\pi}|\mathbf{m}|^2 \tag{30}$$

For a single magnetic dipole at resonance (i.e., $b_1 = 1$) and outside the lattice, for a plane wave excitation, and exploiting Equations (2) and (30), the Cartesian scattering cross-section turns to[107,108]

$$\sigma_{\mathrm{sca},0}^{\mathrm{c}}\left(\tilde{\Lambda} = \infty\right) = \frac{6\pi}{k^2} = \frac{3\lambda^2}{2\pi} \tag{31}$$

and, now, for the meta-atom inside the lattice[109]

$$\frac{\sigma_{\mathrm{sca}}^{\mathrm{c}}\left(\tilde{\Lambda} \approx 0.2, 0.8\right)}{\sigma_{\mathrm{sca},0}^{\mathrm{c}}\left(\tilde{\Lambda} = \infty\right)} = \left(\frac{4\pi\tilde{\Lambda}^2}{3}\right)^2 \approx 0.02, 7.18 \tag{32}$$

It is clear from the results that at the two resonances, one can achieve much weaker (at $\tilde{\Lambda} \approx 0.2$) or more substantial (at $\tilde{\Lambda} \approx 0.8$) scattering cross-section in comparison to the response of the isolated object.

3.5. Fully Diffracting Metagratings

This subsection demonstrates the applicability of the analytical expressions from Table 2A to a design challenge. We seek a non-absorbing metagrating that diffracts all the light to a polar angle of $\theta = 64°$ into the first diffraction orders, or for modes for which it holds $|n_1| + |n_2| = 1$, and with no other propagating modes. The goal of the design process is presented in **Figure 5**a. Note that for the first diffraction orders, there are four distinct branches with azimuth angles of $\phi = 0°, 90°, 180°, 270°$, or, alternatively, the diffraction order pairs, $(n_1, n_2) = \{(1, 0), (-1, 0), (0, -1), (0, 1)\}$. For each of the four branches, two different polarizations are possible, TE and TM. However, due to the isotropy of the constituents and lattice symmetry, some modes are zero. Herein, without losing generality, we have assumed a TE polarized plane wave excitation at normal incidence.

As presented in the equation in Table 2A.3, for normal incidence, or, $\theta_{\mathrm{inc}} = 0$, the diffraction angles (θ, ϕ) are uniquely determined by the diffraction order pair (n_1, n_2). For a set diffraction angle of $\theta = 64°$, the required normalized periodicity is, then, calculated as $\tilde{\Lambda} = \Lambda/\lambda = 1$. Note, that the 2D array lattice dimension is not subwavelength. In the next step, using the analytics expressions in Table 2A for the amplitudes of the diffraction modes, we seek to find the required Mie coefficients that suppress the amplitude into the zeroth diffraction order, or $n_1 = n_2 = 0$, transmission. For this purpose, we rely on representing the possible Mie coefficients using the Mie angles.[103] Representing the possible values of the Mie coefficients using the Mie angles allows to systematically search through all possible electric and magnetic dipole and quadrupole Mie coefficients for regimes where the zeroth-order transmission is zero at the fixed periodicity. It should be mentioned that due to the analytic equations at hand, the numerical calculations are

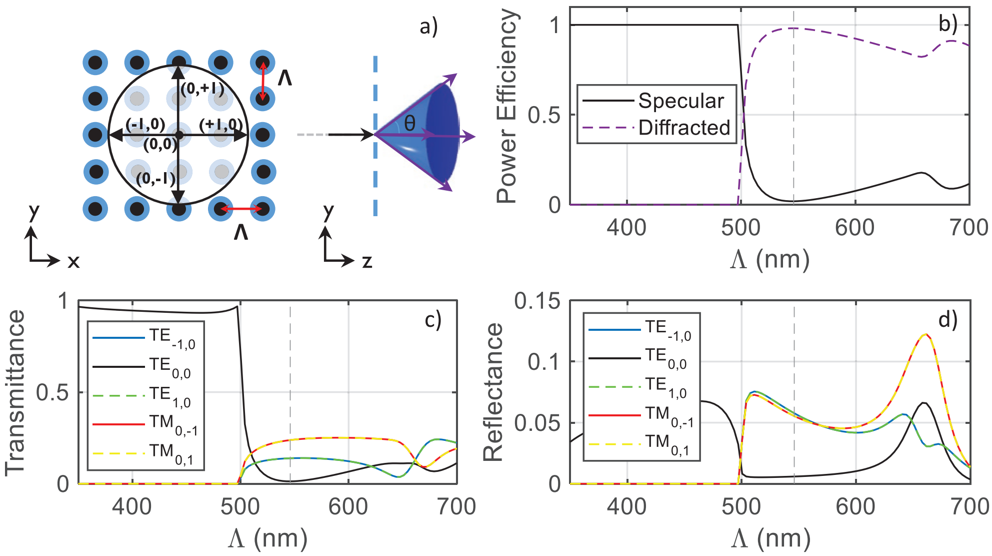

Figure 5. Fully diffracting metagrating. a) A square array of core–shell spheres ($r_{core} = 0.34\lambda$, $r_{shell} = (0.34 + 0.06)\lambda$, $n_{core} = 1.86$, $n_{shell} = 1.43$) illuminated with a TE polarized plane wave at normal incidence shall diffract all the light to the first diffraction orders at an operational wavelength of $\lambda = 500$ nm. b) The lattice's normalized specular and diffracted power as a function of the periodicity Λ. c) The transmittance and d) the reflectance of the zeroth and the higher diffraction orders of the lattice. The dashed line shows the periodicity where diffraction to $\theta = 64°$ occurs.

computationally cheap, and this fosters multidimensional investigation. After the identification of a set of Mie coefficients that cancel the zeroth-order transmission, we use a particle swarm optimization method[104] to find the dimensions and material parameters of a core-shell sphere that provide the required Mie coefficients. At the operational wavelength of $\lambda = 500$ nm, we, finally, find that a core-shell sphere with $r_{core} = 170$ nm, $r_{shell} = 170 + 30$ nm, $n_{core} = 1.86$, and $n_{shell} = 1.43$ satisfies the requirement.

In Figures 5b–d, we show the simulated response of a metagrating made from the designed core-shell spheres arranged in a square array at $\lambda = 500$ nm. Figure 5b shows the power efficiency of the metagrating in diffracting the power at the chosen periodicity $\Lambda = 1.12\lambda = 556$ nm (marked with vertical dashed line). Thus, most of the power is diffracted. Figures 5c,d show the transmittance and reflectance of the individual diffraction orders. The reflectance and transmittance can be expressed as a function of reflection and transmission coefficients, respectively, as

$$T = |t|^2 \frac{|\cos\theta|}{|\cos\theta_{inc}|}, \quad R = |r|^2 \frac{|\cos\theta|}{|\cos\theta_{inc}|} \tag{33}$$

where for our case $\theta = 64°$ and $\theta_{inc} = 0°$. It can be seen that the zeroth-order transmission and the zeroth-order reflection are successfully suppressed at the assigned periodicity. This novel fully diffracting metagrating is a prime example of how our analytic equations are a powerful design tool for on-demand applications.

4. Oblique Incidence: Analytic Equations

4.1. Zeroth-Order Modes of Metasurfaces with Isotropic Dipole Meta-Atoms

Even though metasurfaces have been extensively studied under normal incidence, the oblique incidence is less explored. However, understanding the complete angular response is essential for designing metasurface-based photonic devices.[65] Therefore, this section provides simplified analytical equations to express the optical response of metasurfaces made from dipolar isotropic particles illuminated at oblique incidence. Higher-order expressions for particles with certain symmetries can also be derived from Equation (11).

For the case of an oblique incidence, the symmetry of the lattice coupling matrix changes in comparison to normal incidence, and there are more non-zero elements on the matrix $\bar{\bar{C}}$. Nevertheless, the symmetry of the coupling matrix at oblique incidence is only affected by the lattice type. Therefore, changing the lattice constant or the incidence angles for a specific 2D lattice does not alter the symmetry of the matrix, but only the values of the coefficients. In Figure S4, Supporting Information, we have plotted the Cartesian coupling matrix of an obliquely illuminated square array up to quadrupolar order. Furthermore, the effective polarizability of the Ag-core SiO_2-shell particle considered in Figure 2f inside the square lattice when illuminated at the oblique angle is shown.

The dipolar Cartesian coupling matrix can be written as

$$\bar{\bar{C}} = \begin{bmatrix} C_{xx} & 0 & 0 & 0 & 0 & 0 \\ 0 & C_{yy} & 0 & 0 & 0 & C_{yz} \\ 0 & 0 & C_{zz} & 0 & -C_{yz} & 0 \\ 0 & 0 & 0 & C_{xx} & 0 & 0 \\ 0 & 0 & C_{yz} & 0 & C_{yy} & 0 \\ 0 & -C_{yz} & 0 & 0 & 0 & C_{zz} \end{bmatrix} \tag{34}$$

Now, let us assume that a metasurface consists of isotropic dipoles, and we try to derive the zeroth-order response. In this case, not all the coupling coefficients are relevant; the elements of $\bar{\bar{C}}$ that determine the amplitudes of the propagating diffraction orders of the metasurface made from isotropic dipolar particles are C_{xx}, C_{yy}, C_{zz}, and C_{yz}. Note that for simplicity, we have ignored the "dd" subscript, compared to the previous section, as we anyhow only consider dipolar particles. Prior knowledge of the nonzero and relevant elements of the coupling coefficients for this case of study enables us to construct an analytic model that we can use for the upcoming expressions.

Next, we follow a similar procedure to the normal incidence case of the previous section to derive an analytic equation for the zeroth diffraction order, characterized by $(n_1, n_2) = (0, 0)$, from a metasurface made from dipolar isotropic particles. Additionally, in all the following equations, without losing generality, we assume the azimuthal angle to be zero, that is, $\phi_{\mathrm{inc}} = 0$. Assuming, then, a plane wave oblique incidence, the TE and TM polarizations can be defined as

$$\mathbf{E}_{\mathrm{TM}}^{\mathrm{inc}} = \begin{bmatrix} E_x \\ E_y \\ E_z \end{bmatrix} = E_0 \begin{bmatrix} \cos\theta_{\mathrm{inc}} \\ 0 \\ -\sin\theta_{\mathrm{inc}} \end{bmatrix} \mathrm{e}^{\mathrm{i}(k_x^{\mathrm{inc}} x + k_z^{\mathrm{inc}} z)} \tag{35a}$$

$$\mathbf{E}_{\mathrm{TE}}^{\mathrm{inc}} = \begin{bmatrix} E_x \\ E_y \\ E_z \end{bmatrix} = E_0 \begin{bmatrix} 0 \\ 1 \\ 0 \end{bmatrix} \mathrm{e}^{\mathrm{i}(k_x^{\mathrm{inc}} x + k_z^{\mathrm{inc}} z)} \tag{35b}$$

where $k_x^{\mathrm{inc}} = k\sin\theta_{\mathrm{inc}}$ and $k_z^{\mathrm{inc}} = k\cos\theta_{\mathrm{inc}}$ are the x and z component of the impinging wavevector.

Following Equation (2), the induced multipole moments in each particle for TM polarization as a function of the effective Mie coefficients are derived as

$$\begin{bmatrix} p_x/\varepsilon \\ p_z/\varepsilon \\ \eta m_y \end{bmatrix} = \frac{6\pi\mathrm{i}}{k^3} \begin{bmatrix} a_{1,\mathrm{mod.xx}}\cos\theta_{\mathrm{inc}} \\ -\overset{b_{yy}}{a}_{1,\mathrm{mod.zz}}\sin\theta_{\mathrm{inc}} \\ \overset{a_{zz}}{b}_{1,\mathrm{mod.yy}} \end{bmatrix} E_0 \tag{36a}$$

Similarly, for TE polarization, the following relation can be derived for the effective dipole moments

$$\begin{bmatrix} p_y/\varepsilon \\ \eta m_x \\ \eta m_z \end{bmatrix} = \frac{6\pi\mathrm{i}}{k^3} \begin{bmatrix} \overset{b_{zz}}{a}_{1,\mathrm{mod.yy}} \\ -b_{1,\mathrm{mod.xx}}\cos\theta_{\mathrm{inc}} \\ \overset{a_{yy}}{b}_{1,\mathrm{mod.zz}}\sin\theta_{\mathrm{inc}} \end{bmatrix} E_0 \tag{36b}$$

For a normal incidence excitation, that is, $\theta_{\mathrm{inc}} = 0$, the induced moments are the same as what we derived in Equation (18). However, at oblique incidence, the main difference is the induced moments normal to the metasurface plane. These exited moments bring about novel interference patterns not seen at $\theta_{\mathrm{inc}} = 0$ incidence. We will explore, later on, how these normal moments modify the optical response of a metasurface. The effective dipolar polarizabilities of the particles in Equation (36) depend on a) the modulation of the elements with the coupling coefficients C_{xx}, C_{yy}, and C_{zz} and b) the coupling with other multipole moments through the C_{yz} coefficient. The b_{yy} shows the coupled parameters, and the coupling term is written inside the circle. Electric (magnetic) dipole moments are coupled to magnetic (electric) dipole moments. The effective Mie coefficients are, therefore, expressed as

$$\frac{1}{a_{1,\mathrm{eff.yy}}} = \frac{1}{\overset{b_{zz}}{a}_{1,\mathrm{mod.yy}}} = \frac{1 - C_{\mathrm{yz}}^2 b_{1,\mathrm{mod.zz}} a_{1,\mathrm{mod.yy}}}{a_{1,\mathrm{mod.yy}}\left(1 - C_{\mathrm{yz}} b_{1,\mathrm{mod.zz}} \sin\theta_{\mathrm{inc}}\right)} \tag{37a}$$

$$\frac{1}{b_{1,\mathrm{eff.yy}}} = \frac{1}{\overset{a_{zz}}{b}_{1,\mathrm{mod.yy}}} = \frac{1 - C_{\mathrm{yz}}^2 a_{1,\mathrm{mod.zz}} b_{1,\mathrm{mod.yy}}}{b_{1,\mathrm{mod.yy}}\left(1 - C_{\mathrm{yz}} a_{1,\mathrm{mod.zz}} \sin\theta_{\mathrm{inc}}\right)} \tag{37b}$$

$$\frac{1}{a_{1,\mathrm{eff.zz}}} = \frac{1}{\overset{b_{yy}}{a}_{1,\mathrm{mod.zz}}} = \frac{1 - C_{\mathrm{yz}}^2 b_{1,\mathrm{mod.yy}} a_{1,\mathrm{mod.zz}}}{a_{1,\mathrm{mod.zz}}\left(1 - C_{\mathrm{yz}} b_{1,\mathrm{mod.yy}} \csc\theta_{\mathrm{inc}}\right)} \tag{37c}$$

$$\frac{1}{b_{1,\mathrm{eff.zz}}} = \frac{1}{\overset{a_{yy}}{b}_{1,\mathrm{mod.zz}}} = \frac{1 - C_{\mathrm{yz}}^2 a_{1,\mathrm{mod.yy}} b_{1,\mathrm{mod.zz}}}{b_{1,\mathrm{mod.zz}}\left(1 - C_{\mathrm{yz}} a_{1,\mathrm{mod.yy}} \csc\theta_{\mathrm{inc}}\right)} \tag{37d}$$

while the modulated Mie coefficients are calculated as

$$\frac{1}{a_{1,\mathrm{mod.}\nu\nu}} = \frac{1}{a_1} - \mathrm{i}C_{\nu\nu}, \quad \frac{1}{b_{1,\mathrm{mod.}\nu\nu}} = \frac{1}{b_1} - \mathrm{i}C_{\nu\nu} \tag{38}$$

where a_1 and b_1 are the Mie coefficient of the isolated scatterer and $\nu = \{\mathrm{x, y, z}\}$. If we follow a procedure similar to the one performed for normal incidence, the zeroth-order reflection and transmission coefficients of a dipolar metasurface under normal incidence can be calculated. The resulting formulas are provided in Table 2B.

The analytical equations for the transmission and reflection of an obliquely incident metasurface enable efficient and more accessible exploration of the physics involving metasurface structure. In the following subsections, we derive a particular Brewster angle for a single metasurface and further explore the transmission through a Huygens' metasurface under oblique incidence.

Note that higher-order analytic equations, that is, involving quadrupoles, can also be derived from equations in Table 1. However, in this contribution, we focus on the simpler dipolar expressions for the oblique case. If a particular application for a specific scenario is demanded, other analytic equations can be further derived.

4.2. Brewster Angle: Particle-Independent Polarization Filter

As a direct application of the analytic equations for metasurfaces under oblique incidence presented in Table 2B, we can search for specific metasurfaces that offer a desired and predefined optical response. Polarization, for example, is a crucial property of light, and its control is a fundamental necessity for wave modulation. A question at hand concerns the Brewster angle for metasurfaces. The Brewster angle is the angle at which the reflection for TM or TE polarization vanishes.[110–112] Therefore, it provides an important tool to separate different polarizations of light. In this subsection, we provide an example to demonstrate the strength of the analytical equations in finding important regimes for on-demand applications. Here, the set goal is to give the recipe for a metasurface that can separate the two polarizations in reflection. First, we assume a metasurface consisting of only isotropic magnetic dipolar scatterers, or equivalently $a_{n>0} = b_{n>1} = 0$. Magnetic dipoles constitute the lowest-energy resonance in homogeneous high-refractive-index spheres and are easier to achieve. From the equations in Table 2B, the reflection coefficient for such a metasurface can be written as

$$\begin{bmatrix} r_{\mathrm{TE}_{0,0}\to\mathrm{TE}_{0,0}} \\ r_{\mathrm{TM}_{0,0}\to\mathrm{TM}_{0,0}} \end{bmatrix} = \frac{3}{4\pi\tilde{\Lambda}^2\,|\cos\theta_{\mathrm{inc}}|} \times \begin{bmatrix} b_{1,\mathrm{mod.xx}}\cos^2\theta_{\mathrm{inc}} - b_{1,\mathrm{mod.zz}}\sin^2\theta_{\mathrm{inc}} \\ -b_{1,\mathrm{mod.yy}} \end{bmatrix} \tag{39}$$

The equation above shows that the moment induced normal to the metasurface interferes destructively with the moment induced in-plane. To derive the Brewster angle, one needs to find the metasurface parameters where reflection vanishes for the TE polarization. Therefore, the Brewster angle condition further simplifies to

$$\begin{aligned} r_{\mathrm{TE}_{0,0}\to\mathrm{TE}_{0,0}} &= 0 \Rightarrow \\ b_{1,\mathrm{mod.xx}}\cos^2\theta_{\mathrm{inc}} &= b_{1,\mathrm{mod.zz}}\sin^2\theta_{\mathrm{inc}} \Rightarrow \\ \frac{\cos^2\theta_{\mathrm{inc}}}{1/b_1 - \mathrm{i}C_{zz}} &= \frac{\sin^2\theta_{\mathrm{inc}}}{1/b_1 - \mathrm{i}C_{xx}} \end{aligned} \tag{40}$$

At an incidence angle of $\theta_{\mathrm{inc}} = \pi/4$, the Brewster condition becomes independent of the scatterer's Mie coefficient, and thus, simplifies to $C_{xx} = C_{zz}$. In other words, at an oblique incidence angle of 45°, a metasurface can separate the two polarizations irrespective of its constituents, as far as the dipolar approximation holds and the condition mentioned above is satisfied. Sweeping through the lattice constants, we find out that for a Brewster angle of 45 degrees, the required lattice constant is

$$\frac{\Lambda_{\theta_B=\pi/4}}{\lambda} = 0.5352 \tag{41}$$

which is smaller than the dimension where the first diffraction order appears for this incidence angle (i.e., $\tilde{\Lambda} = 0.58$) and, hence, no diffraction occurs.

Therefore, a metasurface at a normalized periodicity of 0.5352 suppresses the reflection for TE polarization as far as the spheres are small enough compared to the operational wavelength to be described with a magnetic dipole response. The reflected amplitude for the other polarization can be determined via Equation (40) by the strength of the effective magnetic Mie coefficient. A similar Brewster angle can be derived to suppress reflection in TM polarization, that is, the s-polarization, with a metasurface made from electric dipolar particles at the same normalized periodicity point of operation.

Using the analytical formulas of Equation (40), we can, generally, derive the condition for the Brewster angle for different metasurfaces, depending on combinations of the Mie coefficients and the lattice dimension. Here, we demonstrated a simple but powerful case.

4.3. Huygens' Metasurfaces under Oblique Angle

Huygens' metasurfaces have attracted significant attention in the optics community due to their ability to provide unity transmittance, and broad phase coverage.[3,32,74–76,113] Although Huygens' metasurfaces are extensively studied at normal incidence, the oblique incidence case is not well studied yet,[114,115] the main reason potentially being the lack of analytical tools. Questions of retaining the unity transmittance or additionally providing a phase coverage are still under-explored.

This subsection, shortly, studies the transmission of Huygens' metasurfaces in the subwavelength regime, depending on the lattice constant and the incidence angle. The Huygens' metasurface we study is made from dipolar isotropic particles at resonance when considered isolated (i.e., $a_1 = b_1 = 1$). **Figure 6** shows the amplitude and phase of transmission versus the normalized periodicity and the angle of incidence via the formulas of Table 2B. The dashed line shows the onset of the first diffraction order. We ignore the results above this dashed line to assure a single-mode operation.

For a Huygens' metasurface, due to the electromagnetic duality symmetry of its constituents, both TE and TM excitations result in the same reflection and transmission.

When illuminated at normal incidence, or $\theta_{\mathrm{inc}} = 0$, regardless of the polarization, transmission amplitude is 1, as seen from

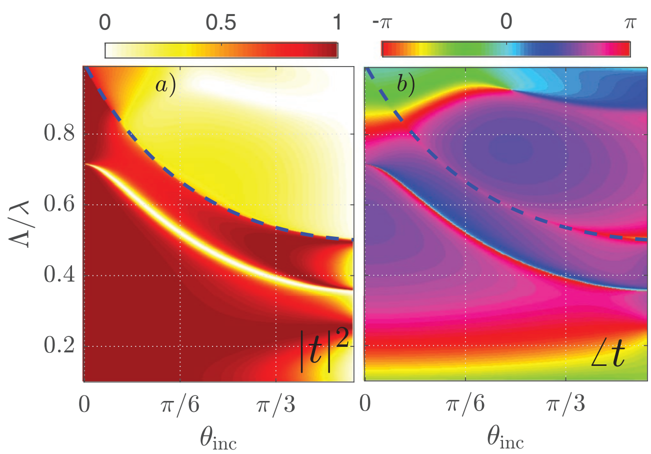

Figure 6. Obliquely illuminated Huygens' metasurface: a) The transmittance and b) phase of the zeroth-order transmission coefficient of a Huygens' metasurface as a function of the incident angle θ_{inc} and the normalized periodicity Λ/λ. The metasurface is made from a particle with an isolated electric and magnetic Mie coefficient of 1, that is, at resonance ($a_1 = b_1 = 1$). The dashed blue line indicates the onset of diffraction orders. Note that for a Huygens' metasurface, the TE and TM excitations are equivalent.

Figure 6a. Furthermore, a broad phase shift coverage of almost $3\pi/4$ is achievable when changing the normalized periodicity in the range [0.7,1].[16] If different but equal electric and magnetic Mie coefficients are considered, the periodicity range in which a broad phase coverage is accessible changes. Therefore, depending on the particle size and the permissible densities, a proper point of operation can be chosen for the metasurface.

For those currently chosen Mie coefficient values ($a_1 = b_1 = 1$), it is apparent from the results in Figure 6, that for small oblique incidence (i.e., $\theta_{\mathrm{inc}} < \pi/6$), the broad phase coverage range (i.e., $\Delta(\angle t) > \pi$) falls, primarily, into the regime for which the metasurface is diffracting, and hence the transmission is suppressed. Therefore, we find out that for a better phase coverage with high transmittance under oblique incidence, one must carefully choose a different Mie coefficient to avoid the diffracting region and the sharp zero-transmittance resonance.

If the incidence is only slightly tilted at a normalized periodicity of 0.71, a sharp resonance appears in the transmittance of the metasurface. This resonance can be traced back to the destructive interference of the in-plane and out-plane induced moments, as described previously. Although the sudden drop of the transmittance may spoil the functionality of a Huygens' metasurface for its phase coverage, the prior information of the regime in which it occurs can help avoid this point of operation. Moreover, this interesting region for a metasurface can be exploited in other applications in which normal transparency and oblique opacity are sought after.

In short, our analytic tool can help in designing a Huygens metasurface for a specific application, avoiding the certain undesired point of operations.

5. Conclusion

This paper provides exact, robust, and accessible equations to calculate the amplitudes of all propagating diffraction orders from a 2D lattice decorated with identical but otherwise arbitrarily shaped particles. We provided explicit expressions in both Cartesian and spherical bases up to the octupolar order. By utilizing the polarizability/T matrix of the individual particles and the lattice coefficients, we calculated the effective polarizability/T matrix of the particles. Besides the primary one, the proposed formulas enable the explicit calculation of the amplitudes of all propagating diffraction orders. In addition, tools for the convenient transformation of the two equivalent bases are also provided. Although the main manuscript is focused on the Cartesian basis, the Supporting Information provides complimentary graphs on the spherical basis.

We investigated the impact of the lattice and that of the decorating particle on the optical response of the metasurfaces. Our analytical framework constitutes an extraordinary tool to disentangle the individual impact. For this purpose, we have introduced the coupling matrix of a 2D lattice and explored it explicitly for square and hexagonal lattices. Moreover, based on the defined bases, symmetries of polarizability and T matrix of isotropic, anisotropic, and helical objects were investigated. Stemming from the symmetry-protected zeros of the particle's polarizability and the lattice' coupling matrix in the Cartesian basis, we introduced simplified, efficient, and closed-form analytical formulas, which we used to conveniently design and explore three contemporary metasurface applications, namely a fully-diffracting metagrating, a polarization filter, and a Huygens' metasurface. In addition, our proposed analytical formulas enabled the investigation of the novel and exciting phenomena of bound states in the continuum and collective lattice resonances.

The authors hope that the techniques proposed herein will allow physicists and engineers to conduct investigations related to metasurface phenomena and propose novel photonic designs. Specifically, the analytical formulas presented herein are accessible for optimization problems and may speed up the optical design process. Our comprehensive multipolar theory not only paves the way for further exploration of the rich physics of metasurfaces but also enables a paradigm shift in designing next-generation optical devices. As far as further endeavors are concerned, the presented work could be expanded to incorporate evanescent modes from the 2D arrays and extract more analytical expressions from the existing general equations for on-demand, specific metasurface applications.

Appendix A: Field Expansion via Spherical Wave Functions

Assume a particle positioned inside an infinite, nonisotropic, linear, homogeneous, and isotropic medium. An electromagnetic field illuminates the particle. The total electric field in the spatial domain outside and around the particle at an angular frequency ω consists of the incident and scattered fields. Each of these fields can be expanded using vector spherical harmonics (VSH) as[47]

$$\mathbf{E}_{\mathrm{inc}}(\mathbf{r}) = \sum_{j=1}^{\infty} \sum_{m=-j}^{j} q_{jm}^{\mathrm{e}} \, \mathbf{N}_{jm}^{(1)}(k\mathbf{r}) + q_{jm}^{\mathrm{m}} \, \mathbf{M}_{jm}^{(1)}(k\mathbf{r}) \tag{A1a}$$

$$\mathbf{E}_{\mathrm{sca}}(\mathbf{r}) = \sum_{j=1}^{\infty} \sum_{m=-j}^{j} b_{jm}^{\mathrm{e}} \mathbf{N}_{jm}^{(3)}(k\mathbf{r}) + b_{jm}^{\mathrm{m}} \mathbf{M}_{jm}^{(3)}(k\mathbf{r}) \tag{A1b}$$

with q_{jm}^{ν} and b_{jm}^{ν}, $j = \{1, 2, 3\}$, $m = \{-j, \ldots, j\}$, $\nu = \{\mathrm{e}, \mathrm{m}\}$, the electric/magnetic incident and scattered field expansion coefficients, respectively. The wavenumber k corresponds to the medium that surrounds the particle, and $r > r_{\mathrm{c}}$, with r_{c} being the radius of the sphere that circumscribes the particle. Moreover, the VSH functions are defined as

$$\mathbf{M}_{jm}^{(l)} = \gamma_{jm} \nabla \times \left[\hat{\mathbf{r}} \, z_j^{(l)}(kr) P_j^m(\cos\theta) \mathrm{e}^{\mathrm{i}m\phi} \right] \tag{A2a}$$

$$\mathbf{N}_{jm}^{(l)} = \frac{1}{k} \nabla \times \mathbf{M}_{jm}^{(l)} \tag{A2b}$$

with

$$\gamma_{jm} = \sqrt{\frac{(2j+1)}{4\pi j(j+1)}} \sqrt{\frac{(j-m)!}{(j+m)!}} \tag{A2c}$$

with $l = 1$ for the incident field and $l = 3$ for the scattered one. $z_j^{(1)}(x) = j_j(x)$ is the spherical Bessel function of the first kind, while $z_j^{(3)}(x) = h_j(x)$ is the spherical Hankel function of the first kind. Finally, $P_j^m(x)$ is the associated Legendre polynomial.

The scattering coefficients can be calculated, using the orthogonality relations, as a function of the incident field via the following formulas,

$$b_{jm}^{\mathrm{e}} = \frac{\int_S \mathbf{N}_{jm}^{(3)}(\hat{\mathbf{r}}) \cdot \mathbf{E}_{\mathrm{sca}}(\hat{\mathbf{r}}) \mathrm{d}S}{\int_S |\mathbf{N}_{jm}^{(3)}(\hat{\mathbf{r}})|^2 \mathrm{d}S} \tag{A3}$$

$$b_{jm}^{\mathrm{m}} = \frac{\int_S \mathbf{M}_{jm}^{(3)}(\hat{\mathbf{r}}) \cdot \mathbf{E}_{\mathrm{sca}}(\hat{\mathbf{r}}) \mathrm{d}S}{\int_S |\mathbf{M}_{jm}^{(3)}(\hat{\mathbf{r}})|^2 \mathrm{d}S} \tag{A4}$$

where the integrating surface S is any sphere enclosing the particle, as shown in Figure 1. Generally, Equation (A3) cannot be calculated analytically, except for simple geometries, like spheres.[116] Therefore, the elements of the T matrix of the particle understudy can be numerically obtained after a series of simulations for a sufficient number of either plane-wave incidences[55] or normalized VSH functions of (A2) as incidence.[56,57] Up to the octupolar order or $N = 3$, which is the limit of this work, the calculation is affordable and adequately fast for most particle geometries with a modern computer. Thus, it is a proper pre-processing step for the 2D array scattering computations performed herein. Moreover, the T matrix calculation is done once. Afterward, metasurface response computations can be performed quickly for various lattice setups, angles of incidence, and frequency ranges via the presented formulas.

Appendix B: Normalized Polarizability and Denormalized Polarizability in SI Units

In this work, the normalized polarizabilities are used in the definition of Equation (2). They are all dimensionless and, hence, can be directly compared to each other. Nevertheless, if the polarizabilities in SI units are required, they can be directly obtained from the normalized ones as

$$\overline{\overline{\alpha}}_{jj'}^{vv'} = \frac{\zeta_j \zeta_{j'}}{k^{j+j'+1}} \overline{\overline{\tilde{\alpha}}}_{jj'}^{vv'} \tag{B1a}$$

$$\zeta_j = \sqrt{(2j+1)!\pi} \tag{B1b}$$

with $\{j, j'\} = \{1, 2, 3\}$ and $\{v, v'\} = \{\mathrm{e}, \mathrm{m}\}$. More information about calculating the prefactors ζ_j can be found in Section S.III, Supporting Information.

Appendix C: Field and Multipole Vector Definitions

The irreducible multipole moment vectors in Equation (2) are defined as

$$\mathbf{p} = \begin{bmatrix} p_x \\ p_y \\ p_z \end{bmatrix} \tag{C1a}$$

$$k\varepsilon^{-1}\mathbf{Q}^{\mathrm{e}} = \frac{k}{\varepsilon\sqrt{3}} \begin{bmatrix} Q_{xy}^{\mathrm{e}} \\ Q_{yz}^{\mathrm{e}} \\ \frac{\sqrt{3}}{2} Q_{zz}^{\mathrm{e}} \\ Q_{xz}^{\mathrm{e}} \\ \frac{1}{2}\left(Q_{xx}^{\mathrm{e}} - Q_{yy}^{\mathrm{e}}\right) \end{bmatrix} \tag{C1b}$$

$$k^2\varepsilon^{-1}\mathbf{O}^{\mathrm{e}} = \frac{k^2\sqrt{6}}{4\varepsilon} \begin{bmatrix} \frac{1}{2}\left(3O_{xx}^{\mathrm{e}} - O_{yy}^{\mathrm{e}}\right) \\ \frac{\sqrt{6}}{4} O_{xyz}^{\mathrm{e}} \\ \frac{\sqrt{15}}{2} O_{yzz}^{\mathrm{e}} \\ \sqrt{\frac{5}{2}} O_{zzz}^{\mathrm{e}} \\ \frac{\sqrt{15}}{2} O_{xzz}^{\mathrm{e}} \\ \frac{\sqrt{6}}{2}\left(O_{zxx}^{\mathrm{e}} - O_{zyy}^{\mathrm{e}}\right) \\ \frac{1}{2}\left(O_{xxx}^{\mathrm{e}} - 3O_{xyy}^{\mathrm{e}}\right) \end{bmatrix} \tag{C1c}$$

while the fields are defined as in Equation (C2)

$$\boldsymbol{E}_1 = \begin{bmatrix} E_x \\ E_y \\ E_z \end{bmatrix}, \quad \boldsymbol{E}_2 = \frac{1}{2\sqrt{3}} \begin{bmatrix} \partial_y E_x + \partial_x E_y \\ \partial_y E_z + \partial_z E_y \\ \sqrt{3}\partial_z E_z \\ \partial_x E_z + \partial_z E_x \\ \partial_x E_x - \partial_y E_y \end{bmatrix} \tag{C2a}$$

$$\boldsymbol{E}_3 = \frac{\sqrt{6}}{24} \begin{bmatrix} \frac{1}{2}\left\{2\partial_{xy} E_x + \left(\partial_x^2 - \partial_y^2\right) E_y\right\} \\ \frac{2}{\sqrt{6}}\left(\partial_{yz} E_x + \partial_{xz} E_y + \partial_{xy} E_z\right) \\ \frac{1}{\sqrt{10}}\left\{\frac{1}{4}\left(2\partial_{xy} - \partial_y^2\right) E_x + \left(\partial_z^2 - \frac{3}{4}\partial_y^2\right) E_y + 2\partial_{yz} E_z\right\} \\ \frac{2}{\sqrt{15}}\left\{-2\partial_{xz} E_x - 2\partial_{yz} E_y + \left(2\partial_z^2 - \partial_x^2 - \partial_y^2\right) E_z\right\} \\ \frac{1}{\sqrt{10}}\left\{\left(\partial_z^2 - \frac{1}{4}\partial_y^2 - \frac{3}{4}\partial_x^2\right) E_x - \frac{1}{2}\partial_{xy} E_y + 2\partial_{xz} E_z\right\} \\ \frac{2}{\sqrt{15}}\left\{2\partial_{xz} E_x - 2\partial_{yz} E_y + \left(\partial_x^2 - \partial_y^2\right) E_z\right\} \\ \frac{1}{2}\left\{\left(\partial_x^2 - \partial_y^2\right) E_x - 2\partial_{xy} E_y\right\} \end{bmatrix} \tag{C2b}$$

with the magnetic multipoles $\mathbf{m}$, $\mathbf{Q}^{\mathrm{m}}$ and $\mathbf{O}^{\mathrm{m}}$ and fields $\mathbf{H}_j, j = \{1, 2, 3\}$, defined in similar fashion as the electric ones above, but with a multiplication with the prefactor $\mathrm{i}\eta$, as in the case of Equation (2).

The components of multipole moment vectors used, herein, and defined in Equation (C1), form an irreducible set of Cartesian multipole moments that are sufficient for the representation of a scatterer's response up to the respective expansion order. We have used the real spherical harmonics corresponding to atomic orbitals, p, d, and f[92] for the combination and order of the vectors. Other irreducible sets of multipole moments can be formed from the quadrupole, and octupolar matrices,[86] depending on the problem under study or for convenience (Section S.IV, Supporting Information).

Appendix D: Radiation Field Definition in Cartesian Coordinates

The scattering far-field from a particle described up to octupolar order in Cartesian coordinates is defined as

$$\mathbf{E}^{\mathrm{c}}(k\mathbf{r}) = \frac{k^2}{4\pi}\frac{e^{\mathrm{i}kr}}{r}\left[\hat{\mathbf{r}}\times\left(\frac{1}{\varepsilon}\mathbf{p}\times\hat{\mathbf{r}}\right)+(\eta\,\mathbf{m}\times\hat{\mathbf{r}}) - \frac{\mathrm{i}k}{6}\hat{\mathbf{r}}\times\left(\frac{1}{\varepsilon}\mathcal{Q}^{\mathrm{e}}\times\hat{\mathbf{r}}\right)-\frac{\mathrm{i}k}{6}(\eta\,\mathcal{Q}^{\mathrm{m}}\times\hat{\mathbf{r}}) - \frac{k^2}{16}\hat{\mathbf{r}}\times\left(\frac{1}{\varepsilon}\mathcal{O}^{\mathrm{e}}\times\hat{\mathbf{r}}\right)-\frac{k^2}{16}(\eta\,\mathcal{O}^{\mathrm{m}}\times\hat{\mathbf{r}})\right] \tag{D1a}$$

$$\hat{\mathbf{r}} = \hat{r}_x\,\hat{\mathbf{x}}+\hat{r}_y\,\hat{\mathbf{y}}+\hat{r}_z\,\hat{\mathbf{z}} = \sin\theta\cos\phi\,\hat{\mathbf{x}}+\sin\theta\sin\phi\,\hat{\mathbf{y}}+\cos\theta\,\hat{\mathbf{z}} \tag{D1b}$$

where $\hat{\mathbf{r}}$ is the position unit-vector.

The components of the vectors $\mathcal{Q}$ and $\mathcal{O}$ are defined as

$$\mathcal{Q}^{\nu}_{\alpha} = \sum_{\beta}\mathcal{Q}^{\nu}_{\alpha\beta}\hat{r}_{\beta} \tag{D2a}$$

$$\mathcal{O}^{\nu}_{\alpha} = \sum_{\beta\gamma}\mathcal{O}^{\nu}_{\alpha\beta\gamma}\hat{r}_{\beta}\hat{r}_{\gamma} \tag{D2b}$$

with $\{\alpha, \beta, \gamma\} = \{x, y, z\}$ and $\nu = \{\mathrm{e,m}\}$. The Cartesian multipole moments $\mathcal{Q}^{\nu}_{\alpha\beta}$ and $\mathcal{O}^{\nu}_{\alpha\beta\gamma}$ are the elements of the 2D quadrupolar and 3D octupolar matrices, respectively, as defined in ref. [86]. The vectors of Equation (D2) are used only for the calculation of the far-field in Equation (D1) and are different from the irreducible Cartesian multipole moment vectors $\mathbf{Q}^{\nu}$ and $\mathbf{O}$ used in this work and defined in Appendix C.

Appendix E: Transformations between Spherical and Cartesian Coordinates for Multipoles and Fields

Following the procedure of ref. [60], the induced Cartesian multipole moments are related to the scattering coefficients of Equation (1) as

$$\varepsilon^{-1}\,\mathbf{p} = \frac{\zeta_1}{\mathrm{i}k^3}\,\overline{\overline{F}}_1\,\mathbf{b}^{\mathrm{e}}_1 \tag{E1a}$$

$$k\varepsilon^{-1}\,\mathbf{Q}^{\mathrm{e}} = \frac{\zeta_2}{\mathrm{i}k^3}\,\overline{\overline{F}}_2\,\mathbf{b}^{\mathrm{e}}_2 \tag{E1b}$$

$$k^2\varepsilon^{-1}\,\mathbf{O}^{\mathrm{e}} = \frac{\zeta_3}{\mathrm{i}k^3}\,\overline{\overline{F}}_3\,\mathbf{b}^{\mathrm{e}}_3 \tag{E1c}$$

with

$$\overline{\overline{F}}_1 = \frac{1}{\sqrt{2}}\begin{bmatrix} 1 & 0 & -1 \\ -\mathrm{i} & 0 & -\mathrm{i} \\ 0 & \sqrt{2} & 0 \end{bmatrix} \tag{E2a}$$

$$\overline{\overline{F}}_2 = \frac{1}{\sqrt{2}}\begin{bmatrix} -\mathrm{i} & 0 & 0 & 0 & \mathrm{i} \\ 0 & -\mathrm{i} & 0 & -\mathrm{i} & 0 \\ 0 & 0 & \sqrt{2} & 0 & 0 \\ 0 & 1 & 0 & -1 & 0 \\ 1 & 0 & 0 & 0 & 1 \end{bmatrix} \tag{E2b}$$

$$\overline{\overline{F}}_3 = \frac{1}{\sqrt{2}}\begin{bmatrix} -\mathrm{i} & 0 & 0 & 0 & 0 & 0 & -\mathrm{i} \\ 0 & -\mathrm{i} & 0 & 0 & 0 & \mathrm{i} & 0 \\ 0 & 0 & -\mathrm{i} & 0 & -\mathrm{i} & 0 & 0 \\ 0 & 0 & 0 & \sqrt{2} & 0 & 0 & 0 \\ 0 & 0 & 1 & 0 & -1 & 0 & 0 \\ 0 & 1 & 0 & 0 & 0 & 1 & 0 \\ 1 & 0 & 0 & 0 & 0 & 0 & -1 \end{bmatrix} \tag{E2c}$$

Note that $\overline{\overline{F}}_j = (\overline{\overline{F}}_j^{-1})^{\dagger}$.

The transformations between Cartesian and spherical magnetic multipole moments are performed similarly, according to the definitions of Equations (1) and (2). Moreover, the local or incident fields on the scatterer are related to the incidence coefficients of Equation (1) as

$$k^{-j+1}\mathbf{E}_j = \frac{1}{\zeta_j}\overline{\overline{F}}_j\,\mathbf{q}^{\mathrm{e}}_j \tag{E3a}$$

$$k^{-j+1}\mathrm{i}\eta\mathbf{H}_j = \frac{1}{\zeta_j}\overline{\overline{F}}_j\,\mathbf{q}^{\mathrm{m}}_j \tag{E3b}$$

Herein, for the sake of simplicity, normalized incident field amplitudes are employed.

The induced multipole moments of a particle in the Cartesian coordinates when illuminated by an incident wave can be calculated as a function of the induced currents, as depicted in Figure 1a. Specifically, the multipoles in Cartesian coordinate up to the quadrupolar order can be calculated via[117]

$$p_{\alpha} = -\frac{1}{\mathrm{i}\omega}\left\{\frac{k^2}{2}\int_V\left[3(\mathbf{r}\cdot\mathbf{J})r_{\alpha}-r^2J_{\alpha}\right]\frac{j_2(kr)}{(kr)^2}\,\mathrm{d}V+\int_V J_{\alpha}\;j_0(kr)\mathrm{d}V\right\} \tag{E4a}$$

$$m_{\alpha} = \frac{3}{2}\int_V(\mathbf{r}\times\mathbf{J})_{\alpha}\frac{j_1(kr)}{kr}\mathrm{d}V \tag{E4b}$$

$$\mathcal{Q}^{\mathrm{e}}_{\alpha\beta} = -\frac{3}{\mathrm{i}\omega}\times\left\{\int_V\mathrm{d}V\left[3(r_{\beta}J_{\alpha}+r_{\alpha}J_{\beta})-2(\mathbf{r}\cdot\mathbf{J})\delta_{\alpha\beta}\right]\frac{j_1(kr)}{kr} + \frac{2j_3(kr)}{kr}\left[\frac{5r_{\alpha}r_{\beta}(\mathbf{r}\cdot\mathbf{J})}{r^2}-r_{\alpha}J_{\beta}-r_{\beta}J_{\alpha}-\mathbf{r}\cdot\mathbf{J}\delta_{\alpha\beta}\right]\right\} \tag{E4c}$$

$$\mathcal{Q}^{\mathrm{m}}_{\alpha\beta} = 15\int_V\left[r_{\alpha}(\mathbf{r}\times\mathbf{J})_{\beta}+r_{\beta}(\mathbf{r}\times\mathbf{J})_{\alpha}\right]\frac{j_2(kr)}{(kr)^2}\,\mathrm{d}V \tag{E4d}$$

where $\{\alpha, \beta\} = \{x, y, z\}$. The connection between the multipole moments defined above in Cartesian coordinates and the multipole moments vectors defined in Equation (C1) is further elaborated in the Supporting Information.

Appendix F: Multipole-to-Field Translation Tensor $\overline{\overline{W}}$ and Coordinates Transformation Tensor $\overline{\overline{R}}$

In Equation (4), the $\overline{\overline{W}}_j$ is defined as

$$\overline{\overline{W}}_j(\theta,\phi)=\begin{bmatrix}\mathbf{W}_j & \mathbf{W}_j' \\ \mathrm{i}\,\mathbf{W}_j' & \mathrm{i}\,\mathbf{W}_j\end{bmatrix} \tag{F1}$$

The elements of the tensor $\overline{\overline{W}}$ for each multipolar order, required for the scattered field calculation in Equations (4) and (7), are given as in

$$\mathbf{W}_1=\begin{bmatrix} e^{-\mathrm{i}\phi}\cos\theta \\ -\sqrt{2}\sin\theta \\ -e^{\mathrm{i}\phi}\cos\theta\end{bmatrix}^T, \qquad \mathbf{W}_1'=\begin{bmatrix} -e^{-\mathrm{i}\phi} \\ 0 \\ -e^{\mathrm{i}\phi}\end{bmatrix}^T \tag{F2a}$$

$$\mathbf{W}_2=\begin{bmatrix} \frac{1}{2}e^{-\mathrm{i}2\phi}\sin 2\theta \\ e^{-\mathrm{i}\phi}\cos 2\theta \\ -\sqrt{\frac{3}{2}}\sin 2\theta \\ -e^{\mathrm{i}\phi}\cos 2\theta \\ \frac{1}{2}e^{\mathrm{i}2\phi}\sin 2\theta\end{bmatrix}^T, \ \mathbf{W}_2'=\begin{bmatrix} -e^{-\mathrm{i}2\phi}\sin\theta \\ -e^{-\mathrm{i}\phi}\cos\theta \\ 0 \\ -e^{\mathrm{i}\phi}\cos\theta \\ e^{\mathrm{i}2\phi}\sin\theta\end{bmatrix}^T \tag{F2b}$$

$$\mathbf{W}_3=\begin{bmatrix} \frac{\sqrt{15}}{4}e^{-\mathrm{i}3\phi}\sin^2\theta\cos\theta \\ \frac{1}{4}\sqrt{\frac{5}{2}}e^{-\mathrm{i}2\phi}\sin\theta(3\cos 2\theta+1) \\ \frac{1}{16}e^{-\mathrm{i}\phi}(\cos\theta+15\cos 3\theta) \\ -\frac{\sqrt{3}}{8}(\sin\theta+5\sin 3\theta) \\ -\frac{1}{16}e^{-\mathrm{i}\phi}(\cos\theta+15\cos 3\theta) \\ \frac{1}{4}\sqrt{\frac{5}{2}}e^{-\mathrm{i}2\phi}\sin\theta(3\cos 2\theta+1) \\ -\frac{\sqrt{15}}{4}e^{-\mathrm{i}3\phi}\sin^2\theta\cos\theta\end{bmatrix}^T \tag{F2c}$$

$$\mathbf{W}_3'=\begin{bmatrix} -\frac{\sqrt{15}}{4}e^{-\mathrm{i}3\phi}\sin^2\theta \\ -\frac{1}{2}\sqrt{\frac{5}{2}}e^{-\mathrm{i}2\phi}\sin 2\theta \\ -\frac{1}{4}e^{-\mathrm{i}\phi}\left(5\cos^2\theta-1\right) \\ 0 \\ -\frac{1}{4}e^{\mathrm{i}\phi}\left(5\cos^2\theta-1\right) \\ \frac{1}{2}\sqrt{\frac{5}{2}}e^{\mathrm{i}2\phi}\sin 2\theta \\ -\frac{\sqrt{15}}{4}e^{\mathrm{i}3\phi}\sin^2\theta\end{bmatrix}^T \tag{F2d}$$

where θ is the polar angle of the wavevector of the respective diffraction order. The vectors $\hat{\theta}$ and $\hat{\phi}$ can be expressed as a function of the vectors $\hat{\mathbf{x}}$, $\hat{\mathbf{y}}$, and $\hat{\mathbf{z}}$ using the tensor $\overline{\overline{R}}$ as

$$\begin{bmatrix}\hat{\theta} \\ \hat{\phi}\end{bmatrix}=\overline{\overline{R}}\begin{bmatrix}\hat{\mathbf{x}} \\ \hat{\mathbf{y}} \\ \hat{\mathbf{z}}\end{bmatrix}=\begin{bmatrix}\cos\theta\cos\phi & \cos\theta\sin\phi & \sin\theta \\ \sin\phi & -\cos\phi & 0\end{bmatrix}\begin{bmatrix}\hat{\mathbf{x}} \\ \hat{\mathbf{y}} \\ \hat{\mathbf{z}}\end{bmatrix} \tag{F3}$$

Appendix G: Transformations between Spherical and Cartesian Coordinates for Scattering and Extinction Cross-Sections

The scattering cross-section, expressed in spherical coordinates, is defined as[47]

$$\sigma_{\mathrm{sca}}^{\mathrm{s}}=\frac{1}{|E_0|^2k^2}\sum_{j=1}^{3}\left(|\mathbf{b}_j^{\mathrm{e}}|^2+|\mathbf{b}_j^{\mathrm{m}}|^2\right) \tag{G1}$$

where $|\cdot|^2$ is the 2-norm of a vector or a matrix. Herein, the multipole order is limited to the octupole or $j = 3$, as it is the scope of this work.

To express σ_{sca} as a function of the multipole moments in Cartesian coordinates, transformations (E1) and (E2) are employed. Therefore, (G1) is rewritten with the multipole moments expressed in Cartesian coordinates, defined in Appendix A. However, for the specific transformation matrices $|F_j^{-1}|^2 = 1$, (G1) can be manipulated further if ζ_j are, also, calculated. Therefore,

$$\begin{aligned}\sigma_{\mathrm{sca}}^{\mathrm{c}}=\frac{1}{|E_0|^2}\Bigg(&\frac{k^4\varepsilon^{-2}}{3!\pi}|\mathbf{p}|^2+\frac{k^4\eta^2}{3!\pi}|\mathbf{m}|^2+\frac{k^6\varepsilon^{-2}}{5!\pi}|\mathbf{Q}^{\mathrm{e}}|^2 \\ &+\frac{k^6\eta^2}{5!\pi}|\mathbf{Q}^{\mathrm{m}}|^2+\frac{k^8\varepsilon^{-2}}{7!\pi}|\mathbf{O}^{\mathrm{e}}|^2+\frac{k^8\eta^2}{7!\pi}|\mathbf{O}^{\mathrm{m}}|^2\Bigg)\end{aligned} \tag{G2}$$

Similarly, the extinction cross-section can be calculated as a function of the multipole moments and the fields represented in Cartesian coordinates. The extinction cross-section, herein up to $j = 3$ order, is defined as[47]

$$\begin{aligned}\sigma_{\mathrm{ext}}^{\mathrm{s}}&=\frac{-1}{|E_0|^2k^2}\Re\left\{\sum_{j=1}^{3}\left[\mathbf{q}_j^{\mathrm{e}}\cdot\mathbf{b}_j^{\mathrm{e},*}+\mathbf{q}_j^{\mathrm{m}}\cdot\mathbf{b}_j^{\mathrm{m},*}\right]\right\} \\ &=\frac{-1}{|E_0|^2k^2}\Re\left\{\sum_{j=1}^{3}\left[\mathbf{q}_j^{\mathrm{e},\mathrm{T}}\mathbf{b}_j^{\mathrm{e},*}+\mathbf{q}_j^{\mathrm{m},\mathrm{T}}\mathbf{b}_j^{\mathrm{m},*}\right]\right\}\end{aligned} \tag{G3}$$

where the superscript * denotes the conjugate operation and the superscript $^{\mathrm{T}}$ denotes the transpose operation. If the transformations Equations (E1)–(E3) are employed, and after the identity $\overline{\overline{F}}_j^{-1,\mathrm{T}}\overline{\overline{F}}_j^{-1,*}=\overline{\overline{I}}$ is utilized, Equation (G3) finally arrives to

$$\begin{aligned}\sigma_{\mathrm{ext}}^{\mathrm{c}}=-\frac{k}{|E_0|^2}\Im\Bigg(&\frac{1}{\varepsilon}\mathbf{E}_1\cdot\mathbf{p}^*+\eta^2\mathbf{H}_1\cdot\mathbf{m}^*+\frac{1}{\varepsilon}\mathbf{E}_2\cdot\mathbf{Q}^{\mathrm{e},*} \\ &+\eta^2\mathbf{H}_2\cdot\mathbf{Q}^{\mathrm{m},*}+\frac{1}{\varepsilon}\mathbf{E}_3\cdot\mathbf{O}^{\mathrm{e},*}+\eta^2\mathbf{H}_3\cdot\mathbf{O}^{\mathrm{m},*}\Bigg)\end{aligned} \tag{G4}$$

The absorption cross-section can be, afterward, calculated from Equations (G2) and (G4), as $\sigma_{\mathrm{abs}} = \sigma_{\mathrm{ext}} - \sigma_{\mathrm{sca}}$.

More information about deriving the formulas of this Appendix can be found in Section S.V, Supporting Information.

Appendix H: Definition of the Mie Angles

Assume that a particle is isotropic and is described by the electric and magnetic Mie coefficients, a_j and b_j, respectively, where $j \in \mathbb{N}$. If the particle is non-absorbing, then the complex-valued Mie coefficients can be represented with a single real valued angle as[103,108,118,119]

$$a_j = \frac{1}{1-\mathrm{i}\tan\theta_{\mathrm{E}j}} = \cos\theta_{\mathrm{E}j}\; e^{\mathrm{i}\theta_{\mathrm{E}j}} \tag{H1}$$

$$b_j = \frac{1}{1-\mathrm{i}\tan\theta_{\mathrm{M}j}} = \cos\theta_{\mathrm{M}j}\; e^{\mathrm{i}\theta_{\mathrm{M}j}} \tag{H2}$$

where $-\pi/2 \leqslant \theta_{\mathrm{E}j} \leqslant \pi/2$ and $-\pi/2 \leqslant \theta_{\mathrm{M}j} \leqslant \pi/2$ are the electric and magnetic (detuning) Mie angles, respectively.[103] The expressions above capture any possible and physically meaningful Mie coefficient values that agree with the optical theorem.

Supporting Information

Supporting Information is available from the Wiley Online Library or from the author.

Acknowledgements

A.R. and T.D.K. contributed equally to this work. The authors acknowledge support by the German Research Foundation through the priority program SPP 1839 Tailored Disorder (CR 3640/7-2 under project number 278747906) and Germany's Excellence Strategy via the Excellence Cluster 3D Matter Made to Order (EXC-2082/1 - 390761711) and by the Carl Zeiss Foundation through the "Carl-Zeiss-Focus@HEiKA." A.R. and A.G.L. acknowledge support from the Karlsruhe School of Optics and Photonics (KSOP). R.A. acknowledges the support of the Alexander von Humboldt Foundation through the Feodor Lynen (Return) Research Fellowship. T.K. acknowledges the support of the Alexander von Humboldt Foundation through the Humboldt Research Fellowship for postdoctoral researchers. A.G.L. acknowledges support from the Max Planck School of Photonics, which is supported by BMBF, Max Planck Society, and Fraunhofer Society. The authors would like to thank Xavier Garcia-Santiago, Ivan Fernandez-Corbaton, Mun Jungho, and Rho Junsuko for the fruitful discussions. The authors are grateful to the company JCMwave for their free provision of the FEM Maxwell solver JCMsuite. R.A. and R.W.B. acknowledge support through the Natural Sciences and Engineering Research Council of Canada and the Canada Research Chairs program.

Open access funding enabled and organized by Projekt DEAL.

Conflict of Interest

The authors declare no conflict of interest.

Data Availability Statement

Research data are not shared.

Keywords

2D lattices, lattice coupling, metasurfaces, polarizability, T matrix

Received: September 24, 2021
Revised: December 3, 2021
Published online:

[1] K. Koshelev, Y. Kivshar, *ACS Photonics* **2020**, *8*, 102.
[2] C.-W. Qiu, T. Zhang, G. Hu, Y. Kivshar, *Nano Lett.* **2021**, *21*, 5461.
[3] I. Staude, J. Schilling, *Nat. Photonics* **2017**, *11*, 274.
[4] S. M. Kamali, E. Arbabi, A. Arbabi, A. Faraon, *Nanophotonics* **2018**, *7*, 1041.
[5] A. I. Kuznetsov, A. E. Miroshnichenko, M. L. Brongersma, Y. S. Kivshar, B. Luk'yanchuk, *Science* **2016**, *354*, aag2472.
[6] N. I. Landy, S. Sajuyigbe, J. J. Mock, D. R. Smith, W. J. Padilla, *Phys. Rev. Lett.* **2008**, *100*, 207402.
[7] R. Alaee, M. Albooyeh, C. Rockstuhl, *J. Phys. D: Appl. Phys.* **2017**, *50*, 503002.
[8] R. Zhao, L. Zhang, J. Zhou, T. Koschny, C. Soukoulis, *Phys. Rev. B* **2011**, *83*, 035105.
[9] T. Kodera, D. L. Sounas, C. Caloz, *Appl. Phys. Lett.* **2011**, *99*, 031114.
[10] H. S. Khaliq, I. Kim, A. Zahid, J. Kim, T. Lee, T. Badloe, Y. Kim, M. Zubair, K. Riaz, M. Q. Mehmood, J. Rho, *Photonics Res.* **2021**, *9*, 1667.
[11] P. Genevet, F. Capasso, *Rep. Prog. Phys.* **2015**, *78*, 024401.
[12] L. Huang, S. Zhang, T. Zentgraf, *Nanophotonics* **2018**, *7*, 1169.
[13] K. E. Chong, I. Staude, A. James, J. Dominguez, S. Liu, S. Campione, G. S. Subramania, T. S. Luk, M. Decker, D. N. Neshev, I. Brener, Y. S. Kivshar, *Nano Lett.* **2015**, *15*, 5369.
[14] F. Zhou, Y. Liu, W. Cai, *Opt. Express* **2013**, *21*, 4348.
[15] X. Ni, A. V. Kildishev, V. M. Shalaev, *Nat. Commun.* **2013**, *4*, 2807.
[16] A. Rahimzadegan, D. Arslan, D. Dams, A. Groner, X. Garcia-Santiago, R. Alaee, I. Fernandez-Corbaton, T. Pertsch, I. Staude, C. Rockstuhl, *Nanophotonics* **2020**, *9*, 75.
[17] P. Lalanne, P. Chavel, *Laser Photonics Rev.* **2017**, *11*, 1600295.
[18] A. Arbabi, Y. Horie, M. Bagheri, A. Faraon, *Nat. Nanotechnol.* **2015**, *10*, 937.
[19] M. Khorasaninejad, F. Aieta, P. Kanhaiya, M. A. Kats, P. Genevet, D. Rousso, F. Capasso, *Nano Lett.* **2015**, *15*, 5358.
[20] D. Lin, P. Fan, E. Hasman, M. L. Brongersma, *Science* **2014**, *345*, 298.
[21] P. R. West, J. L. Stewart, A. V. Kildishev, V. M. Shalaev, V. V. Shkunov, F. Strohkendl, Y. A. Zakharenkov, R. K. Dodds, R. Byren, *Opt. Express* **2014**, *22*, 26212.
[22] M. Khorasaninejad, W. Zhu, K. Crozier, *Optica* **2015**, *2*, 376.
[23] M. Jang, Y. Horie, A. Shibukawa, J. Brake, Y. Liu, S. M. Kamali, A. Arbabi, H. Ruan, A. Faraon, C. Yang, *Nat. Photonics* **2018**, *12*, 84.
[24] D. Arslan, A. Rahimzadegan, S. Fasold, M. Falkner, W. Zhou, M. Kroychuk, C. Rockstuhl, T. Pertsch, I. Staude, unpublished **2021**.
[25] J. Siegel, A. Y. Wang, S. G. Menabde, M. A. Kats, M. S. Jang, V. W. Brar, *ACS Photonics* **2019**, *6*, 2032.
[26] N. Gieseler, A. Rahimzadegan, C. Rockstuhl, *Opt. Express* **2021**, *29*, 21562.
[27] A. Tittl, A. Leitis, M. Liu, F. Yesilkoy, D.-Y. Choi, D. N. Neshev, Y. S. Kivshar, H. Altug, *Science* **2018**, *360*, 1105.
[28] T. Stav, A. Faerman, E. Maguid, D. Oren, V. Kleiner, E. Hasman, M. Segev, *Science* **2018**, *361*, 1101.
[29] K. Wang, J. G. Titchener, S. S. Kruk, L. Xu, H.-P. Chung, M. Parry, I. I. Kravchenko, Y.-H. Chen, A. S. Solntsev, Y. S. Kivshar, D. N. Neshev, A. A. Sukhorukov, *Science* **2018**, *361*, 1104.
[30] G. Yoon, T. Tanaka, T. Zentgraf, J. Rho, *J. Phys. D: Appl. Phys.* **2021**, *54*, 383002.

[31] R. Marqués, F. Martin, M. Sorolla, *Metamaterials with Negative Parameters: Theory, Design, and Microwave Applications*, Wiley Series in Microwave and Optical Engineering, Vol. 183, Wiley, New York **2011**.
[32] A. Epstein, G. V. Eleftheriades, *J. Opt. Soc. Am. B* **2016**, *33*, A31.
[33] M. Chen, E. Abdo-Sánchez, A. Epstein, G. V. Eleftheriades, *Phys. Rev. B* **2018**, *97*, 125433.
[34] C. L. Holloway, A. Dienstfrey, E. F. Kuester, J. F. O'Hara, A. K. Azad, A. J. Taylor, *Metamaterials* **2009**, *3*, 100.
[35] C. L. Holloway, E. F. Kuester, A. Dienstfrey, *IEEE Antennas Wireless Propag. Lett.* **2011**, *10*, 1507.
[36] K. Achouri, M. A. Salem, C. Caloz, *IEEE Trans. Antennas Propag.* **2015**, *63*, 2977.
[37] S. Tretyakov, *Analytical Modeling in Applied Electromagnetics*, Artech House, Norwood, MA **2003**.
[38] V. E. Babicheva, A. B. Evlyukhin, *ACS Photonics* **2018**, *5*, 2022.
[39] A. B. Evlyukhin, V. R. Tuz, V. S. Volkov, B. N. Chichkov, *Phys. Rev. B* **2020**, *101*, 205415.
[40] A. B. Evlyukhin, C. Reinhardt, A. Seidel, B. S. Luk'yanchuk, B. N. Chichkov, *Phys. Rev. B* **2010**, *82*, 045404.
[41] H. K. Shamkhi, A. Sayanskiy, A. C. Valero, A. S. Kupriianov, P. Kapitanova, Y. S. Kivshar, A. S. Shalin, V. R. Tuz, *Phys. Rev. Mater.* **2019**, *3*, 085201.
[42] M. Yazdi, M. Albooyeh, R. Alaee, V. Asadchy, N. Komjani, C. Rockstuhl, C. R. Simovski, S. Tretyakov, *IEEE Trans. Antennas Propag.* **2015**, *63*, 3004.
[43] Y. Ra'di, V. S. Asadchy, S. A. Tretyakov, *IEEE Trans. Antennas Propag.* **2013**, *61*, 4606.
[44] M. B. Ross, C. A. Mirkin, G. C. Schatz, *J. Phys. Chem. C* **2016**, *120*, 816.
[45] Y. Xu, *Appl. Opt.* **1995**, *34*, 4573.
[46] S. Mühlig, C. Menzel, C. Rockstuhl, F. Lederer, *Metamaterials* **2011**, *5*, 64.
[47] M. I. Mishchenko, L. D. Travis, A. A. Lacis, *Scattering, Absorption, and Emission of Light by Small Particles*, Cambridge University Press, Cambridge **2002**.
[48] D. A. Powell, *Phys. Rev. Appl.* **2017**, *7*, 034006.
[49] R. Dezert, P. Richetti, A. Baron, *Opt. Express* **2019**, *27*, 26317.
[50] J. Mun, J. Rho, *Nanophotonics* **2019**, *8*, 941.
[51] J. Mun, S.-W. Moon, J. Rho, *Opt. Express* **2020**, *28*, 36756.
[52] V. S. Asadchy, I. A. Faniayeu, Y. Ra'di, S. A. Tretyakov, *Photonics Nanostruct. - Fundam. Appl.* **2014**, *12*, 298.
[53] X.-X. Liu, Y. Zhao, A. Alù, *IEEE Trans. Antennas Propag.* **2016**, *64*, 2301.
[54] T. D. Karamanos, N. V. Kantartzis, *Prog. Electromagn. Res. B* **2018**, *82*, 93.
[55] M. Fruhnert, I. Fernandez-Corbaton, V. Yannopapas, C. Rockstuhl, *Beilstein J. Nanotechnol.* **2017**, *8*, 614.
[56] G. Demésy, J.-C. Auger, B. Stout, *J. Opt. Soc. Am. A* **2018**, *35*, 1401.
[57] X. G. Santiago, M. Hammerschmidt, S. Burger, C. Rockstuhl, I. Fernandez-Corbaton, L. Zschiedrich, *Phys. Rev. B* **2019**, *99*, 045406.
[58] R. Alaee, C. Rockstuhl, I. Fernandez-Corbaton, *Adv. Opt. Mater.* **2019**, *7*, 1800783.
[59] F. Bernal Arango, T. Coenen, A. F. Koenderink, *ACS Photonics* **2014**, *1*, 444.
[60] J. Mun, S. So, J. Jang, J. Rho, *ACS Photonics* **2020**, *7*, 1153.
[61] R. Alaee, M. Albooyeh, M. Yazdi, N. Komjani, C. Simovski, F. Lederer, C. Rockstuhl, *Phys. Rev. B* **2015**, *91*, 115119.
[62] P. A. Belov, C. R. Simovski, *Phys. Rev. E* **2005**, *72*, 026615.
[63] A. I. Dimitriadis, D. L. Sounas, N. V. Kantartzis, C. Caloz, T. D. Tsiboukis, *IEEE Trans. Antennas Propag.* **2012**, *60*, 5753.
[64] A. I. Dimitriadis, N. V. Kantartzis, T. D. Tsiboukis, C. Hafner, *J. Comput. Phys.* **2015**, *281*, 251.
[65] M. Albooyeh, S. Kruk, C. Menzel, C. Helgert, M. Kroll, A. Krysinski, M. Decker, D. N. Neshev, T. Pertsch, C. Etrich, C. Rockstuhl, S. A. Tretyakov, C. R. Simovski, Y. S. Kivshar, *Sci. Rep.* **2014**, *4*, 4484.
[66] S. S. Kruk, A. N. Poddubny, D. A. Powell, C. Helgert, M. Decker, T. Pertsch, D. N. Neshev, Y. S. Kivshar, *Phys. Rev. B* **2015**, *91*, 195401.
[67] V. E. Babicheva, A. B. Evlyukhin, *Phys. Rev. B* **2019**, *99*, 195444.
[68] V. E. Babicheva, A. B. Evlyukhin, *J. Appl. Phys.* **2021**, *129*, 040902.
[69] D. Beutel, A. Groner, C. Rockstuhl, I. Fernandez-Corbaton, *J. Opt. Soc. Am. B* **2021**, *38*, 1782.
[70] A. Modinos, *Phys. A: Stat. Mech. Appl.* **1987**, *141*, 575.
[71] N. Stefanou, V. Yannopapas, A. Modinos, *Comput. Phys. Commun.* **2000**, *132*, 189.
[72] P. P. Ewald, *Ann. Phys.* **1921**, *369*, 253.
[73] A. Popov, V. Popov, *J. Math. Chem.* **2020**, *58*, 2399.
[74] M. Decker, I. Staude, M. Falkner, J. Dominguez, D. N. Neshev, I. Brener, T. Pertsch, Y. S. Kivshar, *Adv. Opt. Mater.* **2015**, *3*, 813.
[75] X. Chen, P. Yao, in *Metamaterials, Metadevices, and Metasystems 2018*, *Proc. SPIE*, Vol. 10719, SPIE, Bellingham, WA **2018**, p. 1071907.
[76] S. Liu, A. Vaskin, S. Campione, O. Wolf, M. B. Sinclair, J. Reno, G. A. Keeler, I. Staude, I. Brener, *Nano Lett.* **2017**, *17*, 4297.
[77] H. Feshbach, P. M. Morse, M. Michio, *Methods of Theoretical Physics*, Dover Publications, Mineola, NY **2019**.
[78] K. M. McPeak, S. V. Jayanti, S. J. Kress, S. Meyer, S. Iotti, A. Rossinelli, D. J. Norris, *ACS Photonics* **2015**, *2*, 326.
[79] C. Kittel, P. McEuen, *Introduction to Solid State Physics*, 9th ed., Wiley, New Jersey **2018**.
[80] T. Antonakakis, F. I. Baida, A. Belkhir, K. Cherednichenko, S. Cooper, R. Craster, G. Demésy, J. Desanto, G. Granet, B. Gralak, L. Goray, S. Guenneau, L. Li, D. Maystre, A. Nicolet, E. Popov, G. Schmidt, E. Skelton, B. Stout, F. Zolla, B. Vial, *Gratings: Theory and Numeric Applications*, Aix-Marseille University, Provence **2014**.
[81] Y.-L. Xu, *J. Opt. Soc. Am. A* **2013**, *30*, 1053.
[82] A. Moroz, *Opt. Lett.* **2001**, *26*, 1119.
[83] S. Tretyakov, *Philos. Trans. R. Soc., A* **2015**, *373*, 20140362.
[84] R. Alaee, M. Albooyeh, A. Rahimzadegan, M. S. Mirmoosa, Y. S. Kivshar, C. Rockstuhl, *Phys. Rev. B* **2015**, *92*, 245130.
[85] E. Mobini, A. Rahimzadegan, C. Rockstuhl, R. Alaee, *J. Appl. Phys.* **2018**, *124*, 173102.
[86] J. D. Jackson, *Classical Electrodynamics*, Wiley, New York **1999**.
[87] W.-K. Tung, *Group Theory in Physics*, World Scientific, Singapore **1985**.
[88] I. Fernandez-Corbaton, Ph.D. Thesis, Macquarie University, Sydney **2014**.
[89] A. Rahimzadegan, M. Fruhnert, R. Alaee, I. Fernandez-Corbaton, C. Rockstuhl, *Phys. Rev. B* **2016**, *94*, 125123.
[90] COMSOL, Comsol multiphysics **2020**, http://www.comsol.com/products/multiphysics/
[91] S. Burger, L. Zschiedrich, J. Pomplun, F. Schmidt, in *Integrated Photonics and Nanophotonics Research and Applications*, Optical Society of America, Washington, D.C **2008**, p. ITuE4.
[92] C. D. H. Chisholm, *Group Theoretical Techniques in Quantum Chemistry*, Academic Press, New York **1976**.
[93] W. Weber, G. Ford, *Phys. Rev. B* **2004**, *70*, 125429.
[94] A. F. Koenderink, A. Polman, *Phys. Rev. B* **2006**, *74*, 033402.
[95] M. Conforti, M. Guasoni, *J. Opt. Soc. Am. B* **2010**, *27*, 1576.
[96] D. R. Abujetas, J. Olmos-Trigo, J. J. Sáenz, J. A. Sánchez-Gil, *Phys. Rev. B* **2020**, *102*, 125411.
[97] A. Egel, D. Theobald, Y. Donie, U. Lemmer, G. Gomard, *Opt. Express* **2016**, *24*, 25154.
[98] R. Dezert, P. Richetti, A. Baron, *Phys. Rev. B* **2017**, *96*, 180201.
[99] R. J. Bettles, S. A. Gardiner, C. S. Adams, *Phys. Rev. Lett.* **2016**, *116*, 103602.
[100] E. Shahmoon, D. S. Wild, M. D. Lukin, S. F. Yelin, *Phys. Rev. Lett.* **2017**, *118*, 113601.
[101] A. Rahimzadegan, R. Alaee, T. D. Karamanos, R. W. Boyd, C. Rockstuhl, *J. Opt. Soc. Am. B* **2021**, *38*, C217.

[102] A. B. Evlyukhin, C. Reinhardt, U. Zywietz, B. N. Chichkov, *Phys. Rev. B* **2012**, *85*, 245411.
[103] A. Rahimzadegan, R. Alaee, C. Rockstuhl, R. W. Boyd, *Opt. Express* **2020**, *28*, 16511.
[104] K. Y. Lee, M. A. El-Sharkawi, *Modern Heuristic Optimization Techniques: Theory and Applications to Power Systems*, IEEE Press Series on Power Engineering, Vol. 39, Wiley, New York **2008**.
[105] F. G. De Abajo, R. Gómez-Medina, J. Sáenz, *Phys. Rev. E* **2005**, *72*, 016608.
[106] A. D. Utyushev, V. I. Zakomirnyi, I. L. Rasskazov, *Rev. Phys.* **2021**, 100051.
[107] Z. Ruan, S. Fan, *Appl. Phys. Lett.* **2011**, *98*, 2013.
[108] A. Rahimzadegan, R. Alaee, I. Fernandez-Corbaton, C. Rockstuhl, *Phys. Rev. B* **2017**, *95*, 035106.
[109] S. Tretyakov, *Plasmonics* **2014**, *9*, 935.
[110] R. Paniagua-Domínguez, Y. F. Yu, A. E. Miroshnichenko, L. A. Krivitsky, Y. H. Fu, V. Valuckas, L. Gonzaga, Y. T. Toh, A. Y. S. Kay, B. Luk'yanchuk, A. I. Kuznetsov, *Nat. Commun.* **2016**, *7*, 10362.
[111] S. Yin, J. Qi, *Opt. Express* **2019**, *27*, 18113.
[112] C. Wang, Z. Zhu, W. Cui, Y. Yang, L. Ran, D. Ye, *Appl. Phys. Lett.* **2019**, *114*, 191902.
[113] A. E. H. Love, *Philos. Trans. R. Soc. Lond. Ser. A* **1901**, *197*, 287.
[114] D. Arslan, K. E. Chong, A. Miroshnichenko, D.-Y. Choi, D. Neshev, T. Pertsch, Y. Kivshar, I. Staude, *J. Phys. D: Appl. Phys.* **2017**, *50*, 434002.
[115] C. Gigli, Q. Li, P. Chavel, G. Leo, M. L. Brongersma, P. Lalanne, *Laser Photonics Rev.* **2021**, *15*, 2000448.
[116] C. F. Bohren, D. R. Huffman, *Absorption and Scattering of Light by Small Particles*, Wiley, New York **2008**.
[117] R. Alaee, C. Rockstuhl, I. Fernandez-Corbaton, *Opt. Commun.* **2018**, *407*, 17.
[118] H. C. Hulst, H. C. van de Hulst, *Light Scattering by Small Particles*, Dover Publications, Mineola, NY **1981**.
[119] A. García-Etxarri, R. Gómez-Medina, L. S. Froufe-Pérez, C. López, L. Chantada, F. Scheffold, J. Aizpurua, M. Nieto-Vesperinas, J. J. Sáenz, *Opt. Express* **2011**, *19*, 4815.